POLITECNICO
MILANO 1863

SCUOLA DI INGEGNERIA CIVILE,
AMBIENTALE E TERRITORIALE

Spatio-Temporal analysis for drought in Sudan using remote sensing data

TESI DI LAUREA MAGISTRALE IN GEOINFORMATICS ENGINEERING-INGEGNERIA GEOINFORMATICA

Author: **Abubakr Khalid Ahmed Albashir**

Student ID:	10721042
Advisor:	Prof. Maria Antonia Brovelli
Academic Year:	2021-2022

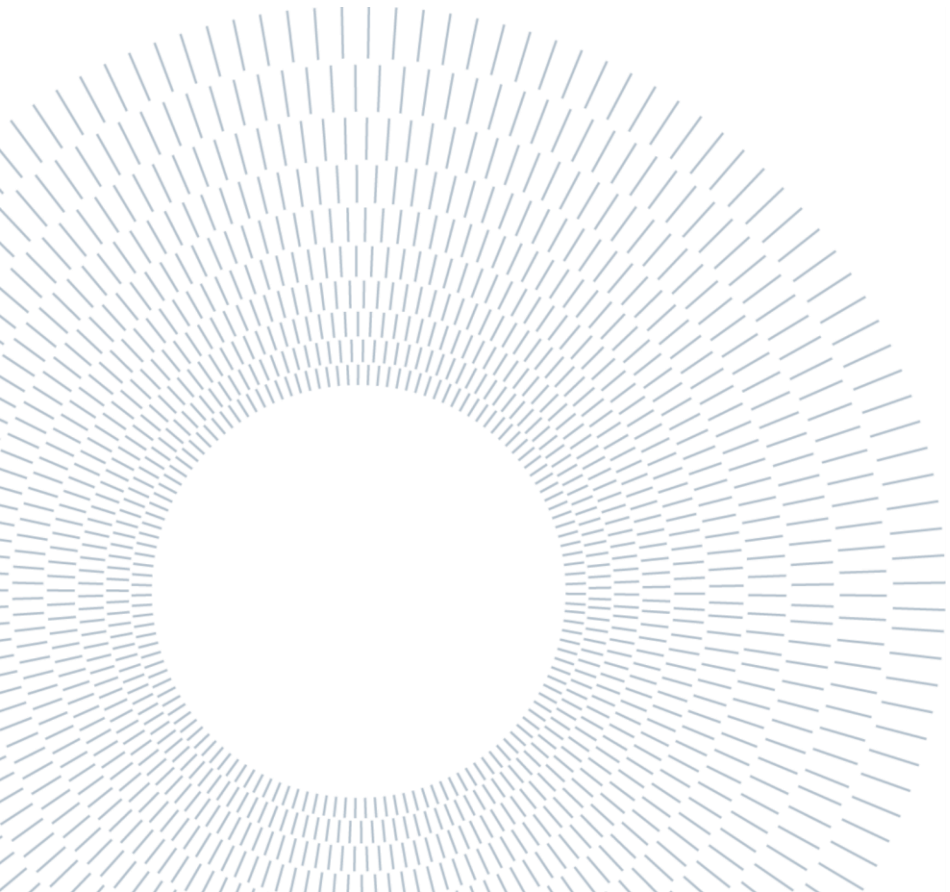

Abstract

Agricultural drought is one of the most severe natural disasters that endanger humans and put food and water security at risk, resulting in a negative impact on livelihoods and the economy.

In Sudan, where the agriculture represents the backbone of the national economy and the dominator of the labor section, the need for continuous and effective monitoring and assessment of the spatial and temporal distribution of the drought and its effect on the agricultural regions is becoming a necessity for the future national and regional related agricultural, social, and economic plans. Such evaluation analysis will assist in development of successful drought mitigation policies.

In this study, we analyzed the spatial and the temporal distribution of the drought on three agricultural regions (Algazeera, North Kurdufan, and Algadaref) states in Sudan over the period between 2009 and 2019.

The NDVI records generated from the MODIS 8-days 250-m and Landsat 7 16-days 30-m were used to derive a linear regression model that describes the relationship between the NDVIs from the two satellites. The linear regression model was then applied on a pixel basis to generate fused NDVI records by blending the MODIS and Landsat NDVI images. The resulted fused NDVI imageries have the temporal resolution of MODIS and the spatial resolution of Landsat and show a high correlation with the MODIS NDVI records over the agricultural regions (0.99, 0.97, and 0.98 in the Algazeera, North Kurdufan, and Algadaref regions respectively).

Subsequently, the Vegetation Condition Index (VCI) was extracted from the three long-term NDVI records, and based on a threshold on the VCI values, monthly and annual mean drought severity and duration maps were generated for the study regions. Furthermore, aggregated drought frequency images were built to define the most vulnerable areas to the drought.

The spatial distribution of the drought maps indicates that each of the three regions was hit by the drought. However, the mean percentages of the affected cropland in the three regions estimated using the Landsat sensor were very close (approximately 15% of the region's cropland in the years where the drought impact was significant and 10% when the drought was light). While the MODIS estimates were far higher (17%, 20%, and 15% in the vulnerable years and 10%, 12%, and 8% in the good vegetation condition years in Algazeera, North Kurdufan, and Algadaref regions respectively), The drought counter images defined the northern parts of North Kurdufan, the eastern parts of Algazeera, and the northern parts of the Algadaref regions as the most vulnerable areas to drought.

The estimated temporal distribution coincided with the national and global records that indicate that the season of 2015 was the strongest drought event. In 2009, the drought was witnessed in both the rainfed and irrigated regions, while the one in the 2011 season was limited to Algadaref and Aljazeera regions. On the contrary, the 2010, 2012, 2016, and 2018 seasons were generally the most drought-resistant years. Throughout the study period, most of the cultivated areas in Algadaref state were hit by the drought.

Moreover, the annual mean VCI maps showed that the agricultural drought had an annual occurrence frequency over the three regions. In addition, the onset of the drought over the analyzed period was detected to be prior to the agricultural season beginning.

The average of the estimated percentage of the population was between 3% and 5% in these two regions, while showing stability in the North Kurdufan region (the percentage of the affected population was below 1.5%).

The findings also demonstrated the potential of the MODIS Land Dynamics dataset to determine cultivation phenological information, the suitability of the Vegetation Condition Index from the three remotely sensed NDVIs in identifying drought onsets, duration, and distribution, and the capability of Landsat-based VCI maps to detect extreme vegetation conditions. As well, the 30-m fused NDVI records, due to their benefit from the higher temporal resolution of MODIS and the higher spatial resolution of Landsat, can be integrated into an early warning and drought monitoring system.

Keywords: Drought monitoring, Spatiotemporal analysis, Sudan, Landsat, MODIS, Drought early warning system.

Abstract in lingua italiana

La siccitàè è uno dei più gravi disastri naturali che mettono a repentaglio la sopravvivenza dell'uomo, compromettendo la sicurezza alimentare e idrica, con un impatto negativo sui mezzi di sussistenza e sull'economia.

Il Sudan é un paese nel quale l'agricoltura rappresenta la spina dorsale dell'economia nazionale, presentandosi come il settore dominante nel mondo del lavoro.

In questo contesto si ha la necessitá, per il futuro nazionale e regionale del paese, di attuare attraverso dei piani agricoli, sociali ed economici, un monitoraggio continuo ed efficace, oltre che una valutazione della distribuzione spaziale e temporale della siccità e dei suoi effetti sulle singole regioni agricole. Tale analisi di valutazione aiuterà lo sviluppo di efficaci politiche di mitigazione degli effetti dovuti alla siccità.

In questo studio, é stata analizzata la distribuzione spaziale e temporale della siccità in tre diversi stati - Algazeera, North Kurdufan e Algadaref- delle regioni agricole in Sudan, nel periodo compreso tra il 2009 e il 2019.

I dati NDVI generati da MODIS (risoluzioni temporale e spaziale: 8 giorni, 250 m) e Landsat 7 (risoluzioni temporale e spaziale: 16 giorni 30-m) sono stati utilizzati per creare un modello di regressione lineare che descriva la relazione tra gli NDVI ottenuti dai due satelliti. Il modello di regressione lineare è stato quindi applicato a livello di pixel per generare dei dati NDVI fusi, partendo da MODIS e Landsat. Le immagini NDVI fuse risultanti hanno la risoluzione temporale di MODIS e la risoluzione spaziale di Landsat e mostrano un'elevata correlazione con il MODIS NDVI nelle regioni agricole (0,99, 0,97 e 0,98 nell'Algazeera, nel Nord del Kurdufan e ad Algadaref).

Successivamente è stato calcolato il Vegetation Condition Index (VCI) dalle tre serie NDVI, e, sulla base di una soglia sui valori VCI mensili e annuali.

per le regioni di studio sono state generate delle mappe di severità e durata media della siccità. Inoltre, sono state costruite immagini aggregate della frequenza della

siccità per definire maggiormente quali siano le zone piú vulnerabili, che sono interessate dalla siccità.

per le regioni di studio sono state generate delle mappe di severità e durata media della siccità. Inoltre, sono state costruite immagini aggregate della frequenza della siccità per definire maggiormente quali siano le zone piú vulnerabili, che sono interessate dalla siccità.

La distribuzione spaziale delle mappe della siccità indica che ciascuna delle tre regioni sono state colpite dalla siccità. Tuttavia, le percentuali medie dei terreni coltivati colpiti dal fenomeno nelle tre regioni, stimate utilizzando il sensore Landsat, erano molto simili (circa il 15% delle terre coltivate della regione negli anni in cui l'impatto della siccità era significativo e il 10% quando la siccità era lieve).

Mentre le stime MODIS erano molto più alte (17%, 20% e 15% negli anni vulnerabili e 10%, 12% e 8% negli anni in buone condizioni di vegetazione rispettivamente delle regioni di Algazeera, Kurdufan settentrionale e Algadaref). Le analisi mostrano che le parti settentrionali del Nord del Kurdufan, le parti orientali di Algazeera e le parti settentrionali delle regioni di Algadaref sono le aree più interessate dalla siccità.

La distribuzione temporale che é stata stimata ha coinciso con i dati nazionali e globali che indicano la stagione del 2015 come l'evento di siccità più forte. Nel 2009 la siccità è stata osservata sia nelle regioni pluviali che irrigate, mentre quella della stagione 2011 è stata limitata alle regioni di Algadaref e Aljazeera. Al contrario, le stagioni 2010, 2012, 2016 e 2018 sono state generalmente gli anni più resistenti alla siccità. Durante tutto il corso del periodo di studio, la maggior parte delle aree coltivate nello stato di Algadaref sono state colpite dalla siccità.

Inoltre, le mappe VCI medie annuali hanno mostrato come la siccità agricola abbia avuto una frequenza annuale nelle tre regioni.

Oltre a ciò, l'esordio della siccità nel periodo analizzato è stata rilevata prima dell'inizio della stagione agricola. La media della percentuale stimata della popolazione era compresa tra il 3% e il 5% in queste due regioni, pur mostrando stabilità nella regione del Kurdufan settentrionale (la percentuale della popolazione colpita era inferiore all'1,5%).

I risultati hanno anche dimostrato il potenziale del set di dati MODIS Land Dynamics per determinare le informazioni fenologiche della coltivazione, l'idoneità dell'indice delle condizioni di vegetazione dei tre NDVI telerilevati nell'identificare l'insorgenza, la durata e la distribuzione della siccità e la capacità delle mappe VCI basate sul Landsat per rilevare condizioni di vegetazione estreme. Inoltre, i dati NDVI fusi di 30 m, grazie al vantaggio della maggiore risoluzione temporale di MODIS e della maggiore risoluzione spaziale di Landsat, possono essere integrati in un sistema di allerta precoce di monitoraggio della siccità.

Parole chiave: monitoraggio della siccità, analisi spaziotemporale, Sudan, Landsat, MODIS, sistema di allerta rapida della siccità.

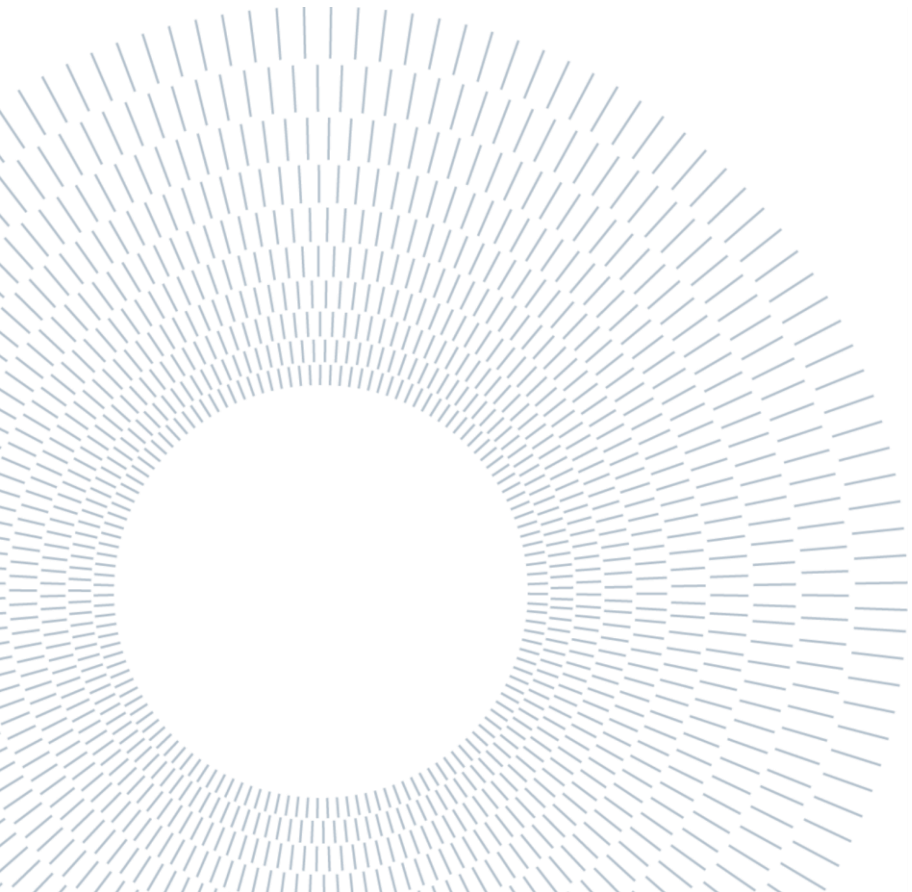

Contents

1. Introduction

In this chapter a general contextual overview, thesis objectives, and the thesis structure will be presented.

1.1 General overview

Sudan is blessed with enormous cultivable land, estimated at 74 million hectares, out of which only some 21.2 million hectares (about 28% in 2018) are currently under cultivation. Agriculture in Sudan is the center of economic activity and people's livelihoods. It meets nearly all of the people's sorghum and millet needs, which make up the majority of the staple food. Furthermore, Sudan's agriculture sector contributes approximately 30% of GDP (2014), provides livelihood to approximately two-thirds of the population, employs approximately 60% [1] of the labor force, and supplies raw materials required by agro-based industries, as well as generates demand for industrial consumer goods.

The ecological system of Sudan's agricultural area can be divided into five vegetation zones based on the rainfall gradient. Starting with the desert in the upper north as part of the largest African desert, then the semi-desert and low-rainfall savannah, and finally the high-rainfall savannah in the south, with the average rainfall increasing southward.

The remote sensing images provide continuously updated source for the environmental phenomenon and had been extensively used for detecting and monitor the drought impact assessment in various ecosystems. In comparison to on-ground measurements, which often require much more effort and are performed on a smaller scale, current operational remote sensing missions, such as Landsat 7 and MODIS, have the advantage of being relatively low-cost, temporally updated, long-term global

observations. The spectral information from the satellite images has been exploited to monitor the vegetation conditions and for agricultural applications such as crop yield monitoring thanks to the Vegetation Indices (VIs). [2]–[4].

The most used vegetation index to describe the vegetation properties is the Normalized Difference Vegetation Index (NDVI), which is based on the Band Ratio Parameter between the Near-Infrared band and the visible red band reflectance. On both local and global scales, NDVI has proven to be a successful quantitative measure of vegetation condition. As well, the NDVI standardized anomalies were studied to detect and monitor the drought impact. [5]–[7]

The Vegetation Condition Index (VCI), derived from the long-term NDVI records, has been designed to enhance the NDVI weather-related component in the NDVI time series and reduce the NDVI noise due to the ecosystem-related component. The bounds of the long-term NDVI records were used as a standard to quantify the extreme vegetation conditions in the study region. VCI has been effectively used for regional analysis of agricultural drought characteristics (onset, duration, intensity, and frequency).

In this study, we investigated the capability of employing the vegetation condition index (VCI) derived from the MODIS and Landsat 7 observations to highlight the agricultural drought characteristics over three agricultural regions (Algazeera, North Kurdufan, and Algadarif) in Sudan during the period between 2009 and 2019. We further improved the analysis by combining the NDVI records from MODIS and Landsat to achieve a fused NDVI that provides reliable and stable data for an early warning system for drought detection and monitoring. Besides, the study assesses the affected population and cropland by the drought during the analyzed period.

1.2 Objectives

The main three objectives of this research can aim at:

1. Investigating the potential of the vegetation condition index derived from multiple remote sensing sensors in highlighting the agricultural drought characteristics over Sudan between 2009 and 2019.

2. Analyzing the agricultural drought impact on the population and croplnad.

3. Assessing the relibility of fused remotely sensed data in improving an early warning system for drought detection and monitoring.

1.3 Thesis structure

The general structure of this thesis can be described as:

- The chapter 2 will give a theretical background about remote sensing and the two main used sensors, as well as the different used data in this project and the study area.

- In chapter 3, the cloud processing platform (Google Earth Engine) and its main architecture will be adressed. Moreover, the adopted methodolgy wil be introduced.

- In chapter 4, the achieved results will be discussed.

- Finally, chapter 5 contains the conculusions, limitations of the study, and the propposed future improvements.

2. Data and study area

This chapter provides an overview of the principles of remote sensing, the used data in the analysis phase of the study as well as the study area.

Remote Sensing is defined as the process of acquiring information about objects from remote positions. This information is retrieved by properly recording and processing the electromagnetic energy emitted or reflected by the investigated objects [8].

2.1 Theoretical Background

2.1.1 Electromagnetic spectrum

Remote sensing term is widely used to refer to the usage of satellite-borne sensors for sensing the Earth's surface for producing thematic maps. The principle of remote sensing is basis on the one of the human eyes vision mechanisms, over and above that, the digital sensors are able to register the light intensity in wider range of the incident light of electromagnetic wave (e.g., infrared, thermal). Hence, the measurement in remote sensing is the electromagnetic waves energy that reflected or emitted by the studied surfaces and recorded by the sensors which are able to register the light radiation intensity of the incident light in a wide range of the electromagnetic wave.

The electromagnetic spectrum is a unidirectional continuous representation of the electromagnetic energy distribution that is ordered by the wavelength (λ) or by the frequency of the wavelength.

Each portion of the electromagnetic spectrum is called a band and this term is often used in remote sensing to describe the sensed reflected light energy within the specific portion of the spectrum.

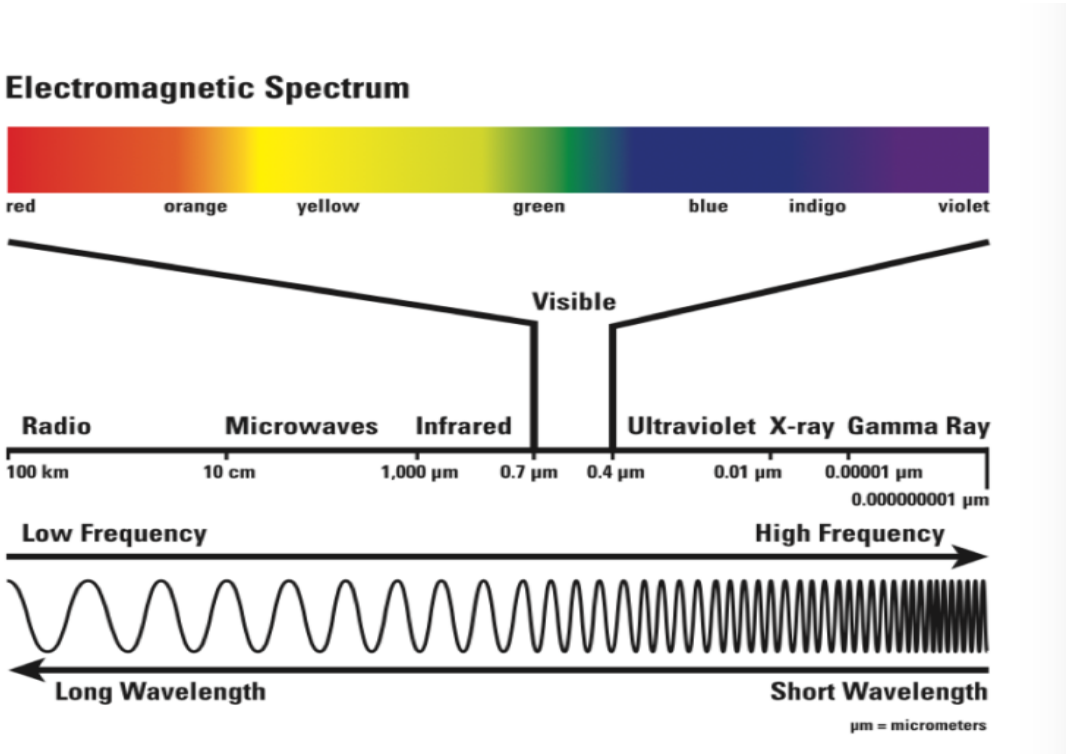

Figure 1. Electromagnetic radiation spectrum used in remote sensing [9].

2.1.2 Spectral signature

Because of the spectral characteristics of the Earth's surface objects, its interaction with the different portions of the light's spectrum might be different. Meaning that the object would absorb or reflect a divergent amount of the light energy regarding the wavelength of the light that it interacted with. This variation in interaction is known as the spectral signature. The spectral signature is a commonly used concept for identifying and detecting the objects on the Earth's surface.

The spectral signatures of numerous ordinary materials, for instance, the water, green vegetation and soil are known and compiled in spectral libraries [10].

Figure 2. below gives an illustration of the spectral signature of the main Earth's surface objects with the light spectrum.

Besides, the spectral signature was the primary principle behind the spectral indices, which are widely used in remote sensing studies and applications.

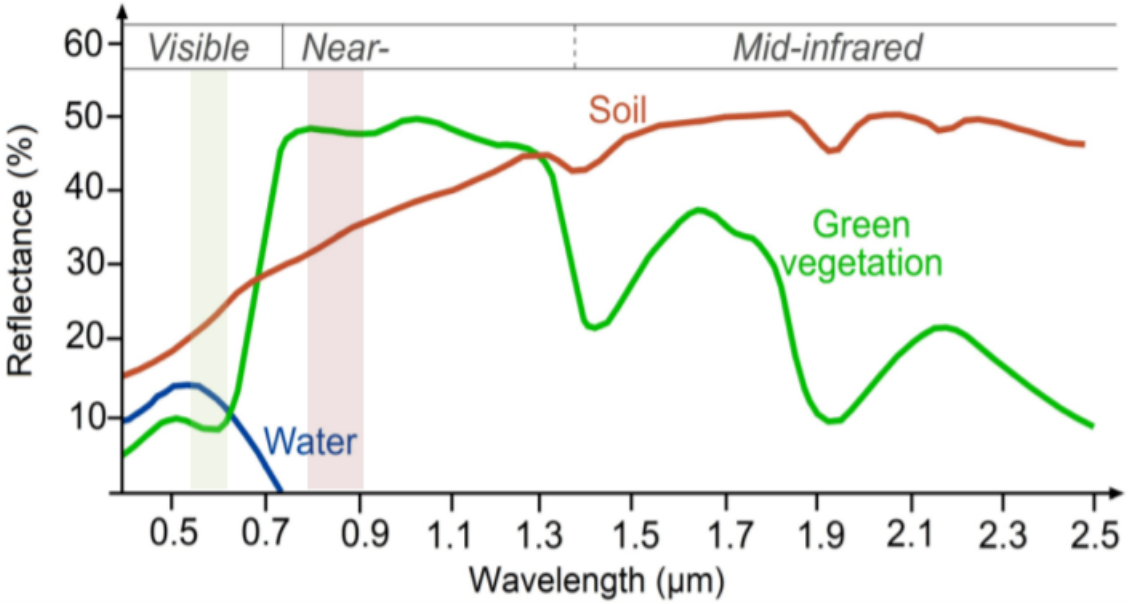

Figure 2. Main Earth's surface object's spectral signature.

2.2 Used data

2.2.1 Landsat 7

One of the Landsat, NASA/USGS program supplies up-to-date most extensive calibrated high-quality Earth's satellite-based images with a moderate resolution catalog since 1972, that provides Earth's observations aims to build Earth's optical images archive all around the world dedicated for environmental monitoring acquires the data by means of the on-board Enhanced Thematic Mapper Plus (ETM+) sensor, an upgraded instrument of the earlier versions of sensing instruments used in Landsat 4 and 5. The mission had been launched in 1999 and it is still dominating the global Earth observation catalog in a 16-day interval of revisiting basis. The images are comprised by eight bands that results of the satellite's sensor capturing for the image footprint in different light portions. The first three bands were captured using the three natural colors channels, Blue, Green and Red in order followed by the near and shortwave Infrared bands.

The advancement in Landsat 7 compared with the Landsat 4 and 5 from spectral bands point of view is the producing of the panchromatic band that had a finer spatial resolution (15 meters).

Since October 2008, USGS made the Landsat data publically accessible for free. Hence, this made the Landsat data one of the essential parts of the Group on Earth Observations (GEO) that met the characteristics set by the United Nations for supporting their Sustainable Development Goals, and therefore, Landsat data is considered as one of the most globally used satellite image observations for environmental monitoring and tracking.

The used collection in this study is the (USGS Landsat 7 Level 2, Collection 2, Tier 1) dataset that had been atmospherically corrected and converted into a surface of reflectance preprocessing level available on the Google Earth Engine platform. The data had been developed with the Landsat Ecosystem Disturbance Adaptive System (LEDAPS) algorithm and delivered along with Quality Assurance (QA) bands (additional bands allow the user to assess the quality of each pixel in the image and to select the pixels that meet the set conditions) and afterward, it packaged into

overlapping scenes with an approximate 170 km x 183 km size of the scene. Table 1. shows the spectral bands of Landsat 7.

	Band name	Wavelength micrometers	Spatial resolution in meters
Band 1	Blue band	0.45 - 0.52	30
Band 2	Green band	0.52 - 0.60	30
Band 3	Red band	0.63 - 0.69	30
Band 4	Near-Infrared band	0.77 - 0.90	30
Band 5	Short-wave Infrared band	1.55 - 1.75	30
Band 6	Thermal band	10.40 - 12.50	60
Band 7	Mid-Infrared band	2.09 - 2.35	30
Band 8	Panchromatic band	0.52 - 0.90	15

Table 1. Spectral bands of Landsat 7 (http://usgs.gov/)

2.2.2 MODIS/ Terra Surface Reflectance 8-Day dataset (MOD09Q1.v0061)

One of the multiple datasets generated from the Terra Moderate Resolution Imaging Spectroradiometer (MODIS) observations gives information of the surface reflectance, the dataset was corrected for the atmospheric effects. For every pixel in the dataset images, a chosen value from all the observations gained over the pixel throughout the 8-day period of acquisition is to be assigned to the pixel.

The standard criteria for the pixel value selection involve the cloud and solar zenith, observation coverage, and the absence of the cloud and shadow.

The dataset has a spatial resolution of 250 m and an approximate scene size of 1200km^2 with global coverage and multi-day temporal resolution. The data is provided in a couple of bands of surface reflectance. These data are mainly used in this study in the analysis phase to extract the monthly MODIS NDVI as well as the main dominator in the 8-day fused NDVI.

2.2.3 MODIS Land Cover Dynamics Yearly 500m Global dataset (MCD12Q2.006)

An annual global land surface dataset that provides valuable information about the vegetation phenological metrics and the seasonal dynamics of the vegetation cover, which gives primary information for agricultural studies. The product was derived from assembling a time series of two bands of Enhanced Vegetation Index (EVI) based on the MODIS nadir bidirectional reflectance distribution function (BRDF)-adjusted reflectance (NBAR) at 500 m spatial resolution [6]. By fitting a cubic smoothing spline to the time series, it allows to identify the valid vegetation cycles within the time series and then extract the phonemetrics of each vegetation cycle.

The valid vegetation cycle is identified as the period of sustained increase in NBAR-EVI2 followed by sustained periods of decrease. Moreover, the peaks in the NBAR-EVI2 time series are detected as points where the first derivative changes sign. These candidate peaks are stored by NBAR-EVI2 magnitude and then analyzed recursively to define the associated start and end dates for the Greenup/down segment [11].

The start of Greenup, MidGreenup and Maturity dates are derived where the NBAR-EVI2 time series crosses 15%, 50%, and 90% of the Greenup segment in NBAR-EVI2 amplitude, respectively. Similarly, Senesece1 and Sensence2 metrics represent the bounds of the growing season as well as the Start Of Season and End Of Season information that determines the beginning and ending period of cultivation.

This dataset is utilized in the cultivation season bounds and their peaks to highlight the interesting time periods over the overall study years.

2.2.4 WorldPop population dataset

A spatial database about the global population in different spatial resolutions (100m, and 1km) is provided by the WorldPop initiative, established in 2013 by combining different regional population mapping projects that aimed to provide informative estimates of the population and their distribution in a gridded base as this data would be a valuable resource of information for research and decision-making.

One advantage of the WorldPop data is that it provides annual estimations of the population. This enables the users to get an updated picture of the population situation. As a result, the data was used by various scientific research to estimate population growth and model the citizens' movement as well as international organizations in humanitarian response to crises. Moreover, the datasets were used in the spatial analysis along with other geospatial data, for instance, to study the distribution of public utilities such as schools and healthcare centers with respect to the local population density. Furthermore, the data was widely used to investigate the impact of the natural disaster and damage analysis.

The WorldPop initiative's population datasets were estimated using recent census-based population data measured on an administrative unit basis, and then it disaggregated these counts into smaller grid cells.

Furthermore, a Random Forest-based machine learning algorithm was used to map the population counts to exploit the spatial pattern similarity and relationships between the population and various geospatial covariate layers.

Hence, the WorldPop dataset with a spatial resolution of 100 m, which is available on Google Earth Engine, was used to estimate the annual number of people affected by agricultural drought in the study area from 2009 to 2019. This rough estimate would provide indicators about the needed actions to mitigate the agricultural drought's impact, as well as allow bridging the gap to achieve the United Nations Sustainable Development Goals (SDGs) 1 and 2, No Poverty, and Zero Hunger in the analyzed regions.

2.2.5 FAO Agricultural Stress Index System (ASIS)

A worldwide monitoring system was developed by FAO to monitor the cultivated areas suffering from severe drought in intense instances using satellite data and then aggregate the results into administrative units. The system provides worldwide information about the vegetation's condition and health in terms of indicators. The system information is composed of two types of indicators:

Seasonal indicators such as the drought detection indices and non-seasonal indicators such as vegetation anomaly indicators. Hence, both types of indicators have been used to validate the agricultural areas and to refine the agricultural mask spatial extent.

2.2.6 Global Food Security-support Analysis Data

A global high-resolution dataset produced by NASA's project aims to provide cropland areas' extent and intensity that contributes toward the global food security and effective cropland mapping.

The GFSAD product is generated by the synthesis of four global cropland products presented by different studies [12] and indicates the cropland since a nominal start year of 2010. The four primary datasets were mainly derived from various remote sensing sensors (e.g., Landsat, MODIS, Geoeye, Quickbird, and RapidEye) as well as ancillary data that included the ASTER-derived Digital Elevation Model (GDEM), historical records of precipitation, and temperature, and digital maps of soil types and administrative units.

The dataset is delivered in a single band called "landcover" that is classified into five classes in order to differentiate between the non-croplands and the cropland regions. In addition, it categorizes the irrigated and rainfed croplands with a nominal spatial accuracy of 1 km.

Table 2. below summarizes the remote sensing datasets used in the analysis phase in this study, besides the time coverage of each data, and its spatial and temporal resolution.

Data	Time period	Spatial resolution	Temporal resolution
Landsat 7 surface reflectance	2009 - 2019	30-m	16-day
MODIS/ Terra surface reflectance	2009 - 2019	250-m	8-day
MODIS Land Cover Dynamics	2009 - 2019	500-m	annually
GFSAD	2007 - 2012	1-km	Multi-year
FAO ASIS dataset	2010 -2019	1-km	annually
WorldPop annual dataset	2009 -2019	100-m	annually

Table 2: Summary of used remote sensing-based datasets in the study.

2.3 Study area

To evaluate the impact of the agricultural drought in Sudan, three regions (Algazeera, North Kordufan and Algadaref) states, shown in Figure 3. below, have been chosen to investigate the effect during the study period on the three different ecosystems and water-feeding ways.

The first region, Al Gezira, is located between the White Nile and the Blue Nile in the east-central of the country and had a mean elevation of 408 m above the mean sea level and contains the world's largest irrigated scheme locates in the center of the country and it depends mainly on the water supply from the Nile River and has two seasons per year. The crops growing in the scheme are cotton, Sorghum, Wheat and Groundnut. The population of the state is about 3.34 million and the average annual rainfall is approximately 283 mm/year [1].

North Kurdufan, the second region in the study area, is located in the West-central region of Sudan between (27 and 32.42 E and 12.21 to 16.51 N) with an average elevation of 490m above the mean sea level and populated by about 1.456 million in 2019 where 79% of the population depends on the agriculture for their livelihood and an annual average of rainfall of respectively low (330 mm/year).

The percentage of the agricultural areas in the region slightly exceeded the quarter of the total area of the state that is (188872 Km^2). The water-feeding method in this region is mainly rain-fed agriculture; therefore, the cultivation has one season annually during the rainfall months. The cultivated crops in the region are sesame, sorghum, and millet.

The third region, Algadaref state, is located in the southeastern part of the country, sharing the international boundaries with Ethiopia and represents one of the biggest agricultural regions in the country. This state is located between (33.58 to 36.56 E and 12.51 to 15.86 N) with a mean elevation of 608m above the mean sea level. The population of the state is about 1.47 Million (2019) and the annual average rainfall estimation is approximately 613 mm/year [1]. Over 74% of the state area (64291 Km^2) is cropland and most of these areas are desert and semi-desert ecological zone while the north part of the state is poor and dense Savanna areas.

The well-known agricultural practices are the traditional and the mechanized ones in the huge, endless individual fields. The most cultivated crops are sesame seeds, sunflower, cotton, and sorghum. The state is the major producer of grains in Sudan, contributing about half of the country's sorghum and millet production. Thus, the state represents the country's granary and it is known as a huge market for crops.

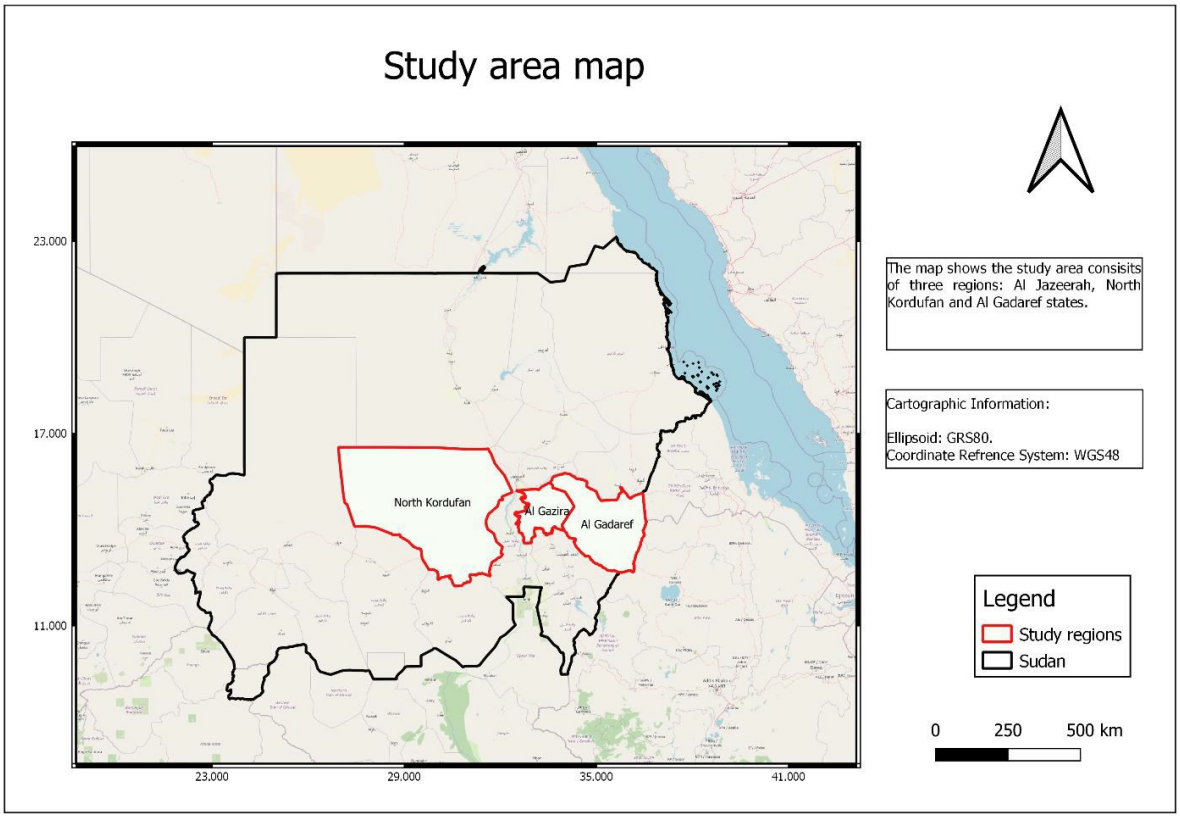

Figure 3. The study area map

The choice of the study regions aims to reflect the impact induced by the agricultural drought in different ecological zones, water-feeding ways and the regional climate so that future mitigation policies can benefit from the study by considering multiple scenarios for agricultural drought detection and monitoring in the country.

The study concentrates on monitoring the agricultural drought-induced over the agricultural areas. Therefore, the croplands over the three study regions have been extracted to define the intended area of interest for the study using different datasets. The main extent of the agricultural mask was provided by the land use office, Ministry of Agriculture in Sudan, in addition to the spatial data provided by the Higher Council for Environment and Natural Resources, Ministry of Environment, Natural Resources

and Physical Development, showing the areas where the governmental agricultural schemes are cultivated, and investors registered in the official governmental records.

Furthermore, the individuals' fields that represent a considerable portion of the croplands had been extracted thanks to the information provided by MIERAG Space Technologies Company, a Sudanese remote sensing company established under the supervision of the Ministry of Science and Technologies, Sudan which is concerned about the national agricultural monitoring using remote sensing data. The spatial information shows the spatial distribution of the cultivated areas since 2009. Then, the provided data has been filtered and validated by the FAO Agricultural Stress Index System (ASIS) data and Global Food Security-support Analysis Data (GFSAD1000) products on the Google Earth Engine. Figure 4. shows the extent of the extracted cropland mask over the study area.

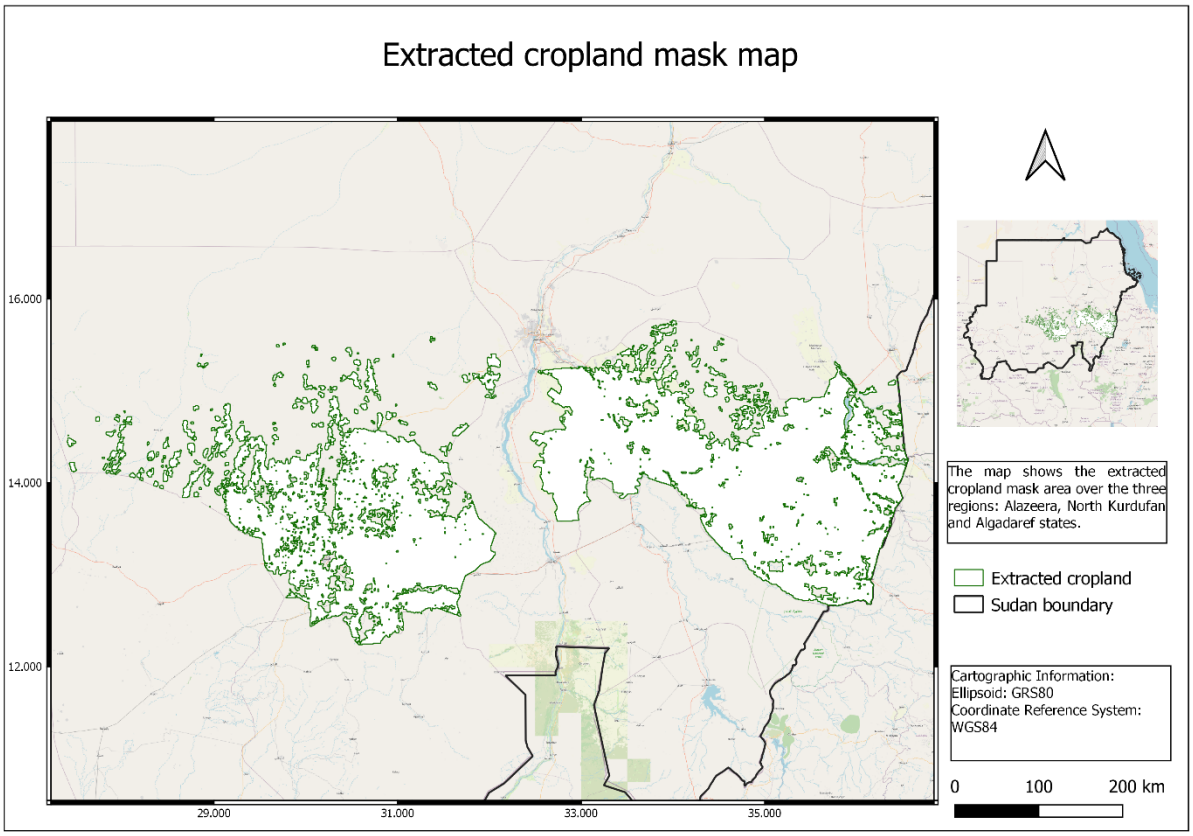

Figure 4. The cropland mask extent map.

3. Processing technology and methodology

In this chapter, the cloud-based processing technology, its architecture, main functionalities, and the ways the user can interact with it will be introduced. As well, the adopted methodology and the analysis steps, including an overview of a proposed fused dataset for an early warning system for drought detection and monitoring, the building of the needed spectral indices objectives, for achieving the study, will be shown.

3.1 Google Earth Engine

The Google Earth Engine is a cloud-based platform with extensive planetary-scale satellite images, Earth observations, and other geospatial data catalogs in an analysis format without the prior need to download [13].

The advantages of using the Google Earth Engine come from many perspectives. First and foremost, the benefits from the publically accessible Earth observations that extend for more than three decades from multiple space agencies and institutes that reach about forty petabytes (i.e., millions of Gigabytes), including Landsat and Sentinel constellation images in different preprocessing levels, multiple MODIS observations and derived products, landcover datasets, and different metrological repositories, just to mention a few, that are continuously updated.

Secondly, the huge server-side leverages Google's server image processing capabilities such as image filtering based on time intervals, cloud coverage, spatial extent, a specific band(s), and other image properties thanks to the platform analysis functionalities. Further, aggregating the analysis results over spatial spaces or over time, which are provided by the platform as well as the interactive web-based code editor, reduces the analysis time and increases the performance, in addition to the

chance of sharing, and reusing the already existing analysis algorithms and adapting them for intended purposes [14].

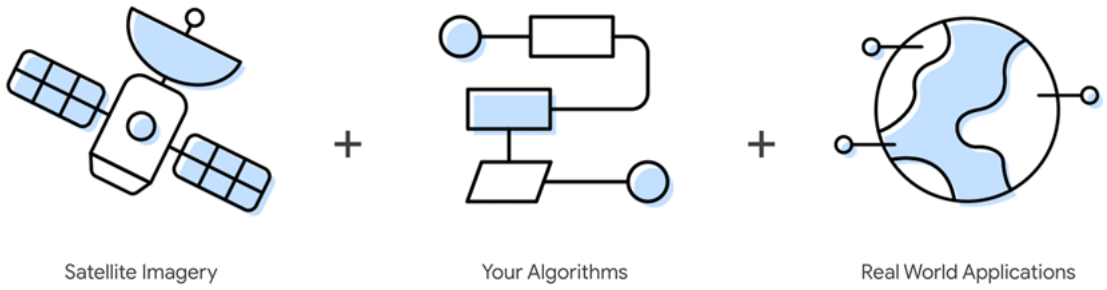

Figure 5. Google Earth Engine overview (https://earthengine.google.com/)

Academically, the Google Earth Engine platform has proved its success in many published academic studies and applications in temporal analysis and environmental tracking on both local and global scales [15], [16]. Google Earth Engine has already introduced simple but powerful APIs (Application Programming Interfaces) available for either Python or JavaScript users through an interactive web-based code editor.

As an online-based platform for global-scale geospatial analysis with huge computational capabilities, GEE can be valuable for analyzing a variety of high-impact societal phenomena such as monitoring forest changes, droughts, hydrogeological disasters, water management, and determining related environmental protection measures [17] since the limited efficiency of the local-machine software makes such analyses impractical, especially for large areas. Thus, the GEE, for its mentioned capabilities, has been chosen as an analysis technology platform for this study.

3.1.1 Google Earth Engine system architecture

The simplified architecture of the system is shown in Figure 6. below. GEE is designed and implemented on top of Google's enabling technologies, along with a web-based database that supports tables of geometric data (points, lines, and polygons).

The first layer is represented by the online code editor, a web-based IDE (Integrated Development Environment), used for writing and deploying simple scripts, and it uses the client libraries to send interactive or batch queries to the system through the REST (Representational State Transfer) API. In the On-The-Fly computation section, the requests by the users are held and distributed to a pool of computation servers. Finally, the data stores contain the images' metadata and enable well-organized selection constraints that can perform the filtering efficiently [18].

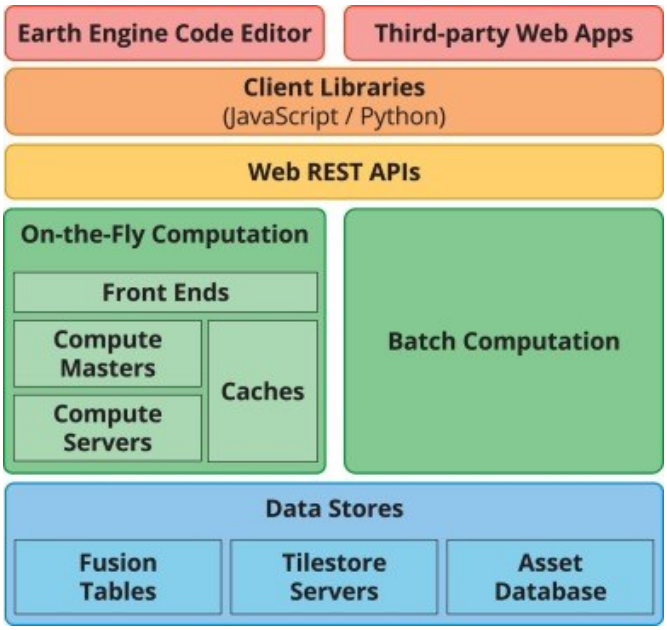

Figure 6. Simplified GEE system architecture [18].

The Google Earth Engine platform provides three different ways that users may interact with the platform. These are: the cloud-editor, the Earth Engine Explorer, and the client libraries.

- The Code editor is a web-based interactive Integrated Development Environment (IDE) that was designed to support JavaScript scripting for retrieving, filtering, and processing data (the already provided data by the platform or the one uploaded by the users). Furthermore, it allows fast data elaboration and simple and effective code-implementation for handling complex geospatial analysis.

- The Earth Engine Explorer: an interface that allows users to interact with the platform's archive of datasets, which includes satellite observations as well as globally convenient derived datasets such as global spectral indices and vector data. The Earth Engine Explorer's data is organized and tagged using keywords that connect similar datasets. Figure 7. illustrates the Earth Engine Explorer and a list of analysis operations through it.

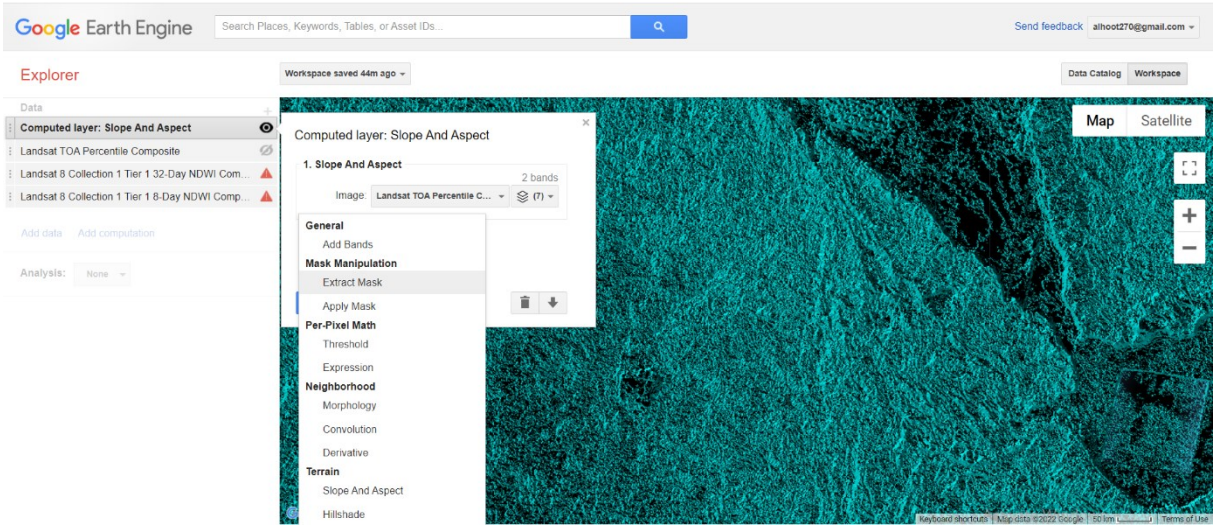

Figure 7. Earth Engine Explorer and a list of available analysis operations

The Earth Engine Explorer is divided into two main sections that the user can browse between; the data catalog, the first, where different datasets are stored; And the workspace, where the analysis is done. The analysis in the workspace is available in a code-free mode, where many simple analysis operations (such as filtering image composites based on a-preferred threshold, and computing slope) are already prepared and, thus, the users can use them without the need to write them.

- Client libraries: a collection of ready-to-use functions, libraries, and wrappers that users can use and/or modify to tailor their proposals and desired analysis. The libraries are available as python or JavaScript-based.

3.2 Methodology

The adopted analysis methodology is described in Figure 8 below. As previously stated, the preprocessing and subsequent analysis steps were carried out in Google Earth Engine.

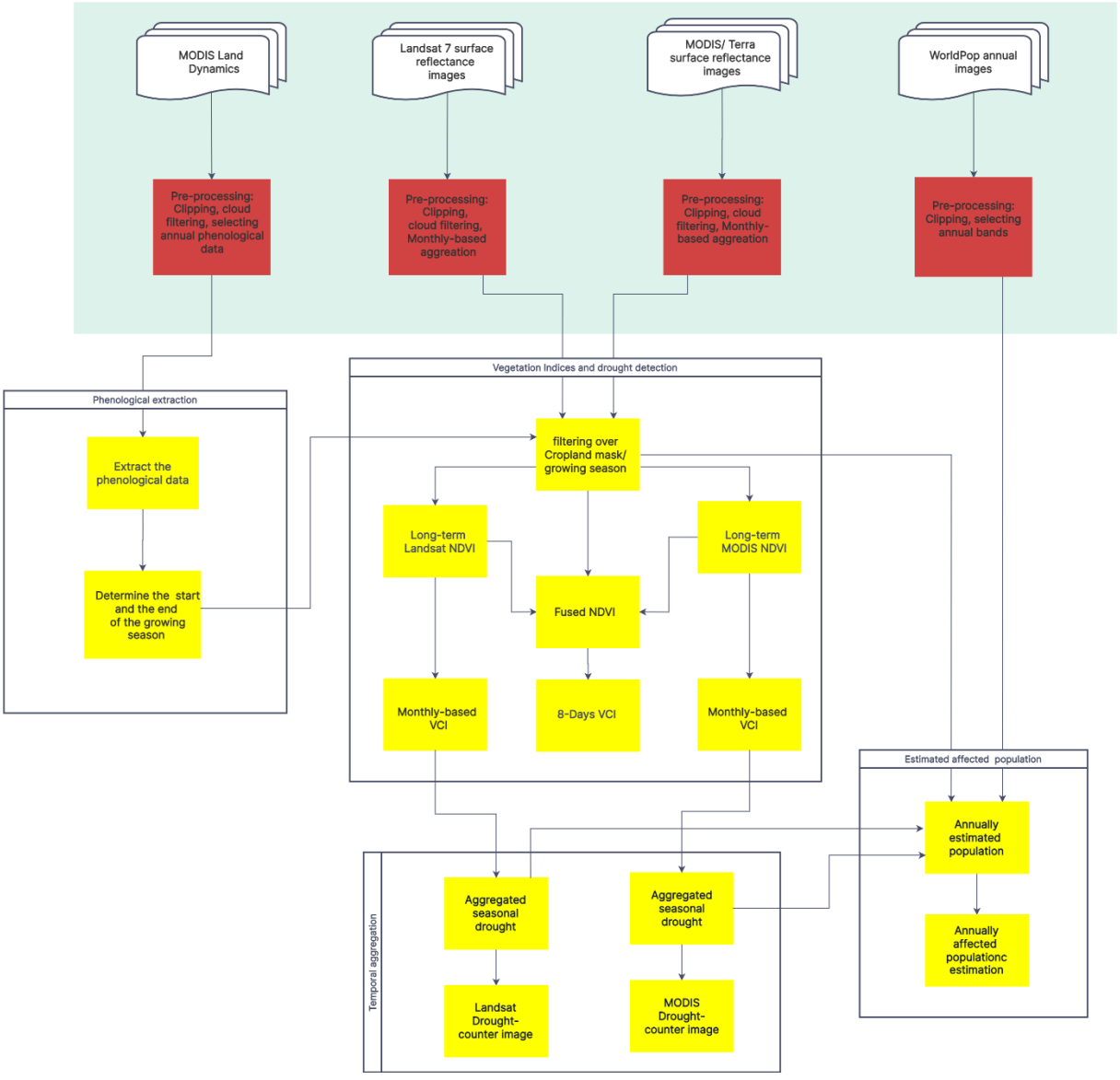

Figure 8. Adopted methodology workflow.

3.2.1 Data preprocessing

Satellite remote sensing Multi-spectral images are mainly collected by sensors from space. This may affect the images due to different kinds of effects it can experience during the image capture due to atmospherical or topographical effects [19]. The process that aims to minimize these effects is called image preprocessing.

For properly multi-spectral remote sensing image analysis results, the image preprocessing step is crucial and may affect the quality of the final results. Thus, in this study, the used datasets were chosen, as described earlier, as atmospherically and topographically preprocessed images.

Upon the image preparation for the analysis phase, only the images with a cloud cover that is less than or equal to 15% of the whole image coverage are considered. This ensures that the validity of the obtained data is not affected by the cloud presence. The images were clipped over the study regions and filtered over the study period.

3.2.2 Agricultural seasons duration determination

Because the study is about agricultural droughts that affect croplands, and because agricultural drought characteristics vary between agricultural seasons [20].

The analysis in each year throughout the study period should be reduced to the cultivation season. Hence, the first step in the analysis was to determine the season timing. This information was also used to inspect how the drought intensity and extent may behave in different ways according to the crop's growing phases.

As emphasized in the data description chapter, MODIS Land Cover Dynamics Yearly Global 500m (MCD12Q2.006) observations were employed to extract the phenological information. The extracted phenological information was:

Number Of Cycles which indicates how many valid vegetation cycles have a peak in a product year, Start Of Season, End Of Season, and Peak Of Season for each region of the three study regions.

From this information, which is mainly in terms of dates, the average Start Of Season, average End Of Season, Peak Of Season, and the duration of the season over each

region were computed. Finally, each of the dates was converted into a Day Of Year (DOY).

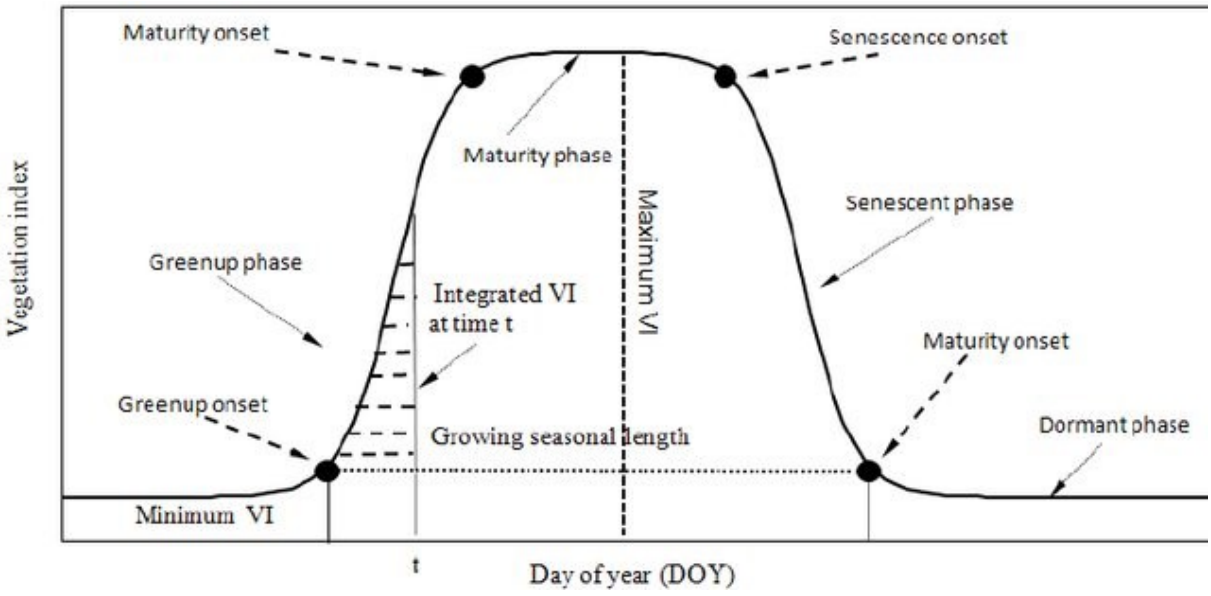

Figure 9. Phenological metrics and their relationship with vegetation index [21].

3.2.3 NDVI (Normalized Difference Vegetation Index)

Vegetation indices are image-based indicators resulting from different band combinations of the same image that show the vegetation properties [22] and thus is widely used for vegetation presence indicators. The vegetation indices are originally derived from the vegetation spectral signature and the vegetation cover interaction with the electromagnetic waves, and thus, they have been used globally to map the vegetation properties [5].

The most well-known vegetation index is the Normalized Difference Vegetation Index (NDVI), which was developed by Rous et al. [23]. as an effective quantitative measure derived from sensor records, and it can be described by the equation (1) below:

$$NDVI = \frac{NIR - R}{NIR + R} \quad (1)$$

Where NIR and R are the spectral reflectance measurements acquired in the Near-Infrared, and the red bands, respectively.

The NDVI formal above shows the difference between the spectral reflectance of the Near-infrared and the red bands using the band ration parameter (BRP) while the normalization in the NDVI formula was introduced to eliminate the seasonal sun angle difference and to minimize the effect of atmospheric attenuation [23].

The NDVI values range between -1 to 1, where the negative values indicate the absence of vegetation cover and the presence of water bodies, while the positive ones represent the presence of vegetation. In sum, the higher the NDVI value, the healthier the vegetation.

The main aim of NDVI is to characterize the vegetation and its health regionally and globally ([6]). Consequently, remote sensing derived NDVI from different missions has rapidly increased in academic research and different related applications since it provides a reliable and continuously updated source of information about vegetation. Besides, NDVI anomalies have been extensively studied to extract information about both the environmental and climatic parameters of vegetation regions [5] and drought detection and monitoring [6], [7].

3.2.4 Data Fusion

The design of any early warning system for drought based on Earth observations mainly relies on the presence of the essential data that is needed for extracting the information about the drought or the indicators of drought.

The main input data for drought detection and monitoring is the satellite-based spectral vegetation indices, hence, the Normalized Difference Vegetation Index (NDVI). Hence, the existence of the two main satellite image providers with adequate spatial and temporal resolution within the region. However, as it was indicated earlier in the description of the used satellite-based imagery datasets in this study, namely; Landsat 7 images provide a 30m resolution that is well-suited for capturing surface spectral reflectance [24], [25] However, Landsat has limited temporal coverage due to its nominally longer revisiting cycle (i.e., 16 days). Furthermore, the regular availability of these data is still questioned in light of cloud contamination and Landsat sensor deterioration as a result of Sensor Scan Line (SCL) failure since 2003 [25], [26].

On the other hand, the used MODIS dataset produces the needed spectral information for generating NDVI with a higher temporal resolution (8-days) composite, which is more suitable for drought analysis from a temporal resolution point of view but with a substandard spatial resolution (250m) that is less suitable for heterogenous cultivated landsacpes [2].

The goal of the multiple satellite sensor data fusion step is to provide superior information and solve problems concerning individual sensors and benefit from their independent advantages. Hereby, in this study, the aim of the data fusion is to produce a synthetic data that has the spatial resolution of the Landsat's as the time-resampling of the MODIS's (i.e., 8 days) in such a way that the result data will have a higher time-frequency as well as a convenient spatial resolution of 30m of Landsat, which is appropriate for the drought mapping details and detecting early warning systems [20], [25].

The input data for the fusion step are the generated Landsat and MODIS NDVI bands resulted from the previous step. Further, the input bands were projected into the same geographic projection (i.e., WGS84).

Based on the assumption made by M. He et al. [2] that the NDVI retrievals from the two different sensor records are consistent and comparable, a pixel-wise linear regression model based on the relation between the two NDVI observations was applied through GEE to mix both Landsat and MODIS NDVI records.

The fused NDVI was derived using the result slope and the intercept from the built linear regression model and the MODIS NDVI data as the equation (2) below:

$$fused_{NDVI} = Intercept + modis_{NDVI} \times slope \quad (2)$$

Where: $fused_{NDVI}$ is the NDVI record resulted from the fusion

$modis_{NDVI}$ is the NDVI record extracted from the MODIS surface reflectance observations.

$Intercept, slope$ are the intercept and the slope of the linear regression model, respectively.

For evaluating the obtained fused NDVI data, the correlation between samples of the fused data and the two original sensors' NDVI records over the three study regions at various time periods was estimated. However, the correlation between the fused and MODIS samples was performed at the same time epochs since both data have the same temporal resolution and, therefore, the same sampling dates. The correlation between the fused and the corresponding Landsat NDVI samples was performed based on the criteria of choosing the fused-Landsat couples who have the least time gaps because the two records, not the necessity, were sampled on the same dates.

3.2.5 Vegetation Condition Index (VCI)

The Vegetation Condition Index was introduced by F.N. Kogan [27]. The main idea is based on the long-term NDVI records. Kogan claims that the NDVI quantifies the spatial difference between the weather component (year-to-year variations in each ecosystem due to weather fluctuations) and the ecosystem component (the productivity of an ecosystem). The weather-related NDVI-component is smaller than the one related to the ecosystem, VCI was mainly designed to reduce the NDVI noise and to enhance the weather-related component in the NDVI time series. Therefore, the normalization can successfully minimize the ecosystem component [28]. Thus, the weather-related NDVI portion can be linearly scaled from zero, minimum NDVI, up to 100, maximum NDVI, for a particular epoch and space unit (e.g., region or grid cell). Consequently, the resulting indicator called the Vegetation Condition Index is defined by the equation (3) illustrated below:

$$VCIi = 100 \times \left(\frac{NDVIi - NDVImin}{NDVImax - NDVImin}\right) \quad (3)$$

Where:

$VCIi$ is the Vegetation Condition Index value of the current epoch

$NDVIi$ represents the NDVI value of the current epoch.

$NDVImin$ is the minimum long-term NDVI value over the vegetation region.

$NDVImax$ is the maximum long-term NDVI value over the vegetation region.

The absolute bounds (maximum and minimum) of long-term NDVI records computed over many years describes the extreme conditions and events and therefore, it can be used as a standard to quantify these extreme conditions [5].

As a result, VCI shows the approximate weather-related component in NDVI, changing from zero, the extremely unfavorable vegetation condition, up to the maximum, 100, showing the optimal vegetation condition compared with historical records of NDVI.

However, Kogan [27] estimated a numerical threshold to define drought events that is less than 40 percent, and a set of VCI values categorizes the drought severity levels [7], [29], as is shown in Table 3. below.

VCI has been effectively used for regional analysis of drought [7], [27], [30]. Hence, the drought detection and monitoring in this study was mainly performed using VCI by means of multiple multi-spectral remote sensing data; MODIS, Landsat, and the fused-NDVI records.

The maximum and minimum NDVI values needed for VCI computation for each sensor's data were extracted from the sensor's historical NDVI data over the study period from 2009 up to 2019. This step was done separately for each of the study regions since the regions have different environmental conditions.

Drought severity level	**VCI Values**
No drought	> 40
Light drought	30 - 40
Moderate drought	20 - 30
Severe drought	10 - 20
Extreme drought	<10

Table 3. shows the Vegetation Condition Index VCI threshold values for drought severity classification.

Hence, the VCI has been calculated over each region using both MODIS and Landsat7 NDVI values on a monthly basis for the duration of the agricultural seasons of the study years to inspect the drought intensity, duration, and spatial extension. Further, the annual average of VCI was calculated to reflect the regions that were hit by drought and the areas that experienced longer events of drought each year.

The fused-NDVI data was employed to investigate the possibility of early drought detection and to show the drought indicators that may not be achieved through the other two sensors. The purpose of using the fused-NDVI data was also to examine the most affected growing period during the growing season.

Because it was far more time-consuming for VCI computation compared with the other two datasets, which may not be an efficient way for the purpose of the early warning system shown in this study, the early drought detection using fused-NDVI was limited to the agricultural season of 2015, the most affected year by the drought throughout the study period.

3.2.6 VCI aggregation over time and space

To understand the temporal evolution of the agricultural drought over time, the results of the computed annual VCI for each of the two satellites, Landsat and MODIS, were aggregated over the study period to estimate the drought occurrence frequency.

This step was performed by producing a binary image considered as a counter for the drought occurrence frequency between 2009 and 2019, over the study region. The binary image cell size was set to be equal to the spatial resolution of the corresponding satellite image. The binary image pixel value was initialized to zero. A drought condition, regardless of its severity level, is identified when the annual VCI lies below the mentioned thresholds in Table 3. Hence, the pixels values of the resulting image (called the drought counter-image) range from zero, where the pixel's footprint experiences no drought event, up to 11, meaning the pixel's footprint was hit by drought annually during the 11 study years.

The drought counter-image can be beneficial for various related sectors (e.g., agricultural, economics, and social planning sectors) and to define the most vulnerable locations for the agricultural drought and can be further analyzed by considering additional agricultural practice information and soil types to access their impact and if these parameters are influential in inducing agricultural drought as well as any possible future adaptation/mitigation policies.

Similarly, the affected areas and their percentage of each of the three regions by the agricultural drought for each of the three study regions were calculated from the computed annual VCI from Landsat and MODIS. This step aims to understand the trend of the agricultural drought impact.

Because most people in agricultural regions rely on agriculture as a source of income [1], any negative impact on agriculture, such as an agricultural drought, will have a

negative impact on the population in these areas. As a result, proper estimation of the number of people affected by the annual drought as well as their distribution, like any other natural disaster, plays a key role in reducing the consequences of the disaster and might even help in enacting effective social policies in the future.

The WorldPop remote sensing data was used to estimate the annual population and its distribution in each of the three interest areas, as well as their percentages of the overall population. For this task, the annual affected cropland areas according to the two sensors, Landsat and MODIS, were used to clip the cropland, then the counts of the population in the clipped regions were estimated. This rough estimate is important in the drought effect analysis because it provides insight into the annual percentage of people affected by agricultural drought.

4. Results and discussion

This chapter concerns the discussion of the achieved results from the analysis methodology discussed in the previous chapter. Hence, the structure of the chapter starts with the determination of the average agricultural season in the three study regions, considering the duration of the study period. Next, the maps showing the Vegetation Condition Index using the main two sensors, Landsat 7 and MODIS, are aggregated on an annual basis for all the years from 2009 to 2019, while the monthly basis is shown only for the most affected years by the drought, namely 2009, 2011, and 2015. Then, the annual percentage of the affected areas and the affected population in each region were illustrated.

The fused derived VCI maps were then shown afterward for 8-day data samples for the agricultural season of 2015, the most vulnerable season.

4.1 Extracting the phenological information and season determination

The phenological information (i.e., the start of season, peak of season, and end of season) was extracted for each vegetation region was extracted from the MODIS land dynamics dataset. This information was given in the form of UNIX dates (the number of seconds elapsed since the 1st of January 1970) and then converted into readable date format. Hereby, the results show the scaled EVI values provided by the same dataset, representing a periodical cycle for each year. Figure 10 shows that the peaks in the seasons approximately coincide with the date of the cycle peaks. Similarly, the start and the end of the seasons are located in the growing and the shrinking phases of the cycle, respectively. One of the considerable notices was that the scaled EVI values were ranged between 0.1 and 0.3, which gives information about the relatively low ecosystem properties. The lowest peaks were found to be in 2015 and 2011, while the highest was found to be in 2012.

The extracted phenological information was averaged over each separate region. The average start of season (SOS) and the average end of season (EOS) for each region were estimated. As Figure 11 shows, the cultivation season starts in the Algazeerah region on average on the 2nd of July and ends on the 21st of October with an average season duration of 111 days. The season in North Kurdufan followed the season in the first region, where it starts in the middle of July, lasts until the 27th of October, and lasts for 104 days.

The agricultural season in the Algadaref region, on the other hand, was estimated to start on the second of August and end on the 16th of November and has a 106-day average.

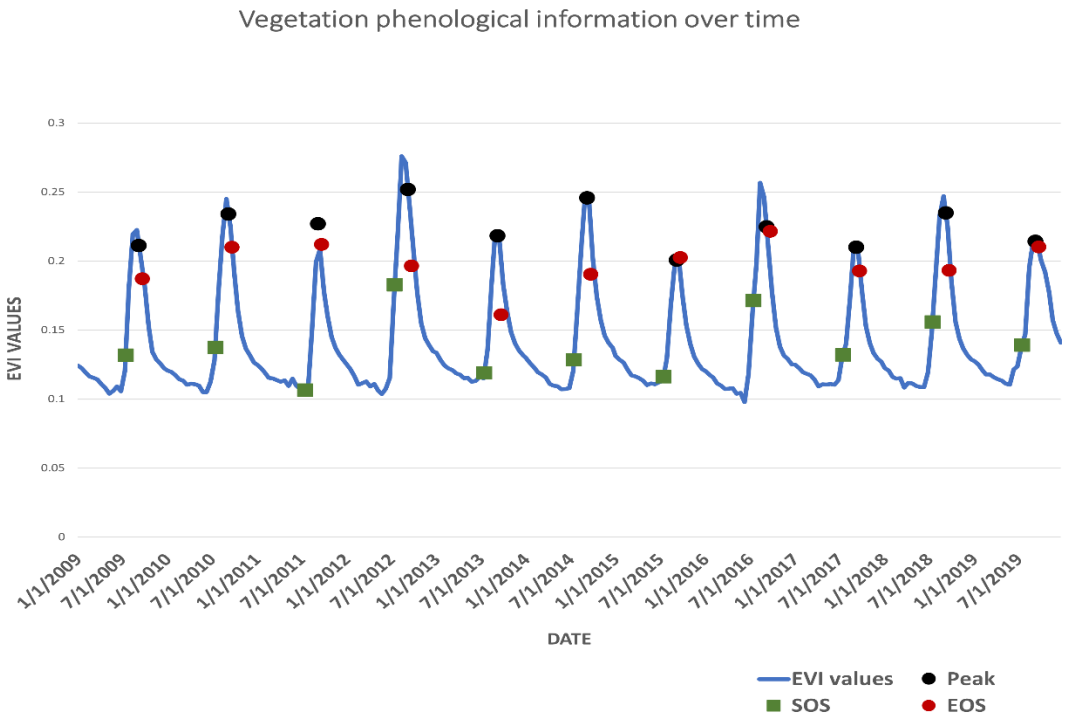

Figure 10. Phenological information extracted in the study area.

The extracted data was then used as a reference for filtering the remote sensing data to exclude the effects of off-season days. A buffer of 16 days was added at the beginning and end of these limits. This is done under the consideration that the sensor images may not be captured exactly on the same day. As a result, the Landsat and MODIS data in this study were filtered over the buffered season period.

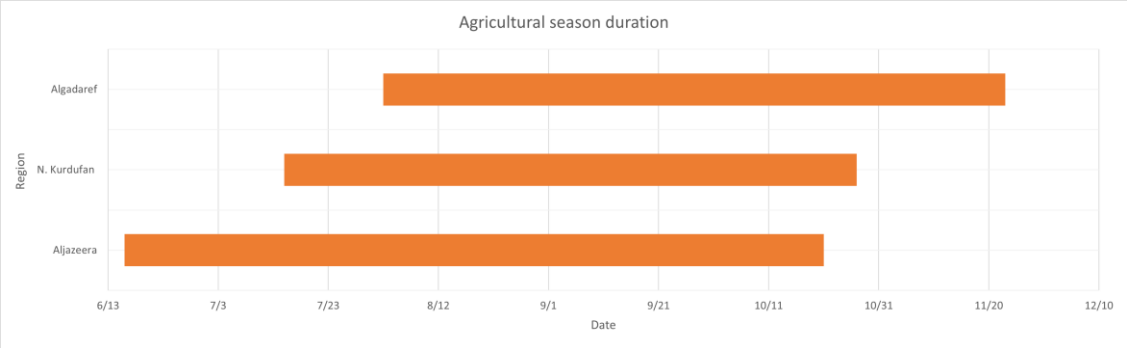

Figure 11. Average agricultural season start and end dates over the study regions.

4.2 Annual mean VCI estimation

The Vegetation Condition Index results over the study regions were estimated using observations acquired through both Landsat 7 and MODIS sensors. Hence, the mean annual maps show the drought intensity and its spatial distribution. The suggested VCI thresholds were used as a drought severity categorization criterion.

According to MODIS annual derived VCIs, the most affected years were 2009, 2011, and 2015. However, the most intense drought occurred in 2015. In these years, as Figure 12, Figure 13, and Figure 14 show, the drought indicators are spatially distributed around the central parts and the northern part of the study regions. In the season of 2015, most of the west region, North Kurdufan, was hit by drought, in addition to the central portion of the rest of the regions, which were affected as well.

Similarly, the Landsat resulting maps, as calculated from VCI, show a very similar pattern to the MODIS one in terms of the affected years and distribution of the drought extent. However, due to its finer spectral and spatial resolution, Landsat VCI maps show much more detailed severity conditions and induced drought distribution. As an example, the 2010 season was estimated by Landsat to have much higher vegetation conditions than the one estimated by the MODIS sensor. This was reflected in the percentage of affected cropland this year. Moreover, during the 2013 and 2017 cultivation seasons, a significant moderate drought that hit most of the Algadaref region was clearly identified by Landsat but was not successfully identified by MODIS derived VCI.

From the VCI maps of the two sensors, it can be recognized that the agricultural drought occurs in all three regions every season, regardless of severity level. According to the Landsat derived maps, in the Algazeerah region, most of the years the induced impact of the agricultural drought on the cropland ranged between 10% and 16% of the agricultural mask and had an average of 10% affected cropland in the drought in the rest of the years. In the North Kurdufan region, a very similar temporal pattern was experienced wherein in the years when the negative impact of drought was significant (2013, 2015, and 2017), the percentage of the affected cropland had slightly exceeded 15% of the total cropland. while it dropped to below 10% of the cropland in the other seasons.

Regarding the Algadaref region, similar to North Kurdufan, the percentage of the affected cropland in 2013, 2015, and 2017 in addition to 2014 was significant and the percentages reached higher than 15% of the cropland in the region. In the other years, the annual drought had less of an impact. However, the least affected cropland was in 2010, where just below 10% of the cropland was affected.

MODIS detected drought frequency follows a similar temporal pattern to Landsat, with all study years experiencing drought of varying severity and spatial distribution. However, regarding the affected cropland areas, they are generally far higher than the estimated affected cropland by Landsat.

During the analyzed period, MODIS data indicates different behaviors of drought while different regions are concerned. In the Algazeerah region, the cropland experienced agricultural drought annually. The percentage of the affected cropland ranges from 10% to 17%. In the years that were significantly hit by the drought (2009, 2017), the percentages reached their peak. The longest moderate drought was identified as the four years from 2009 to 2013. In the North Kurdufan region, the least affected year was 2012, when just 14% of the cropland was hit by the drought. On the contrary, in the rest of the years, the cropland areas were affected by approximately 20% to 25%.

The Algadref region, in contrast, was characterized differently according to MODIS. Hence, the years of good vegetation condition were (2012, 2014, 2016, and 2014) where the percentage of the affected cropland was (11%, 12%, 10%, and 8%) respectively.

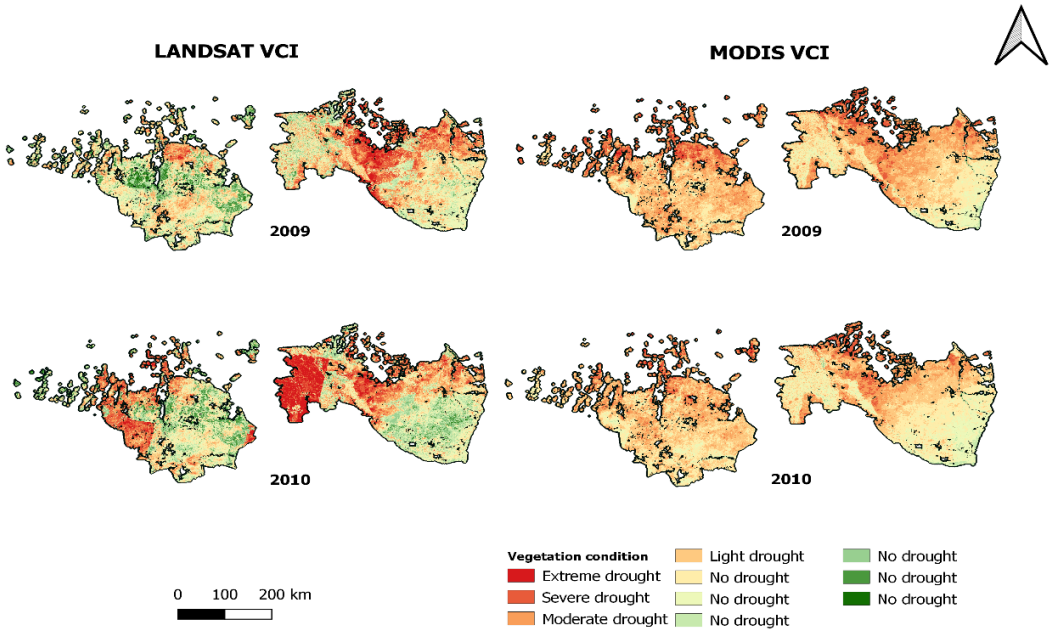

Figure 12. Annual mean VCI using Landsat 7 and MODIS over the study regions during 2009 and 2010

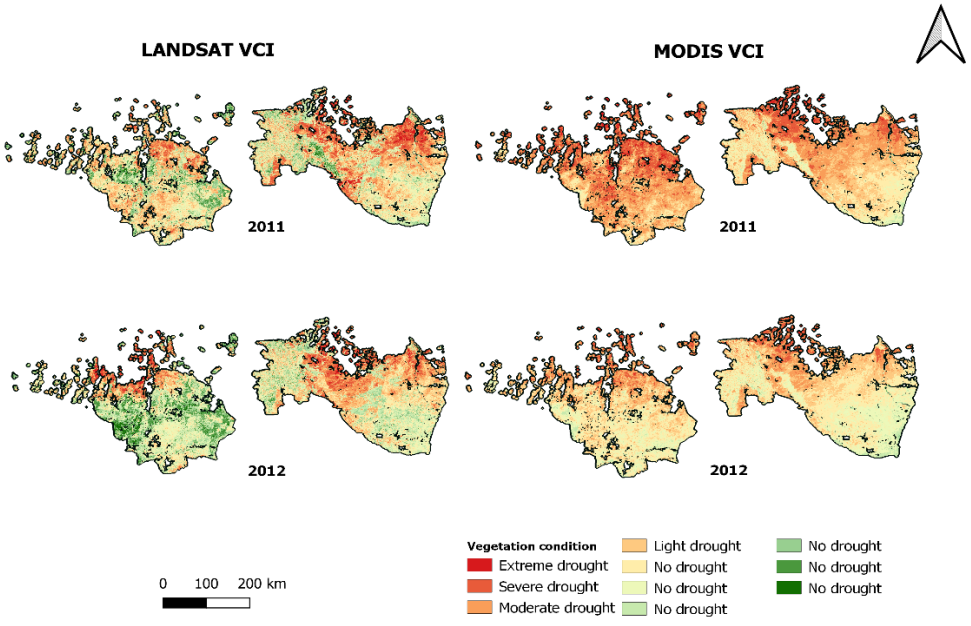

Figure 13. Annual mean VCI using Landsat 7 and MODIS over the study regions during 2011 and 2012

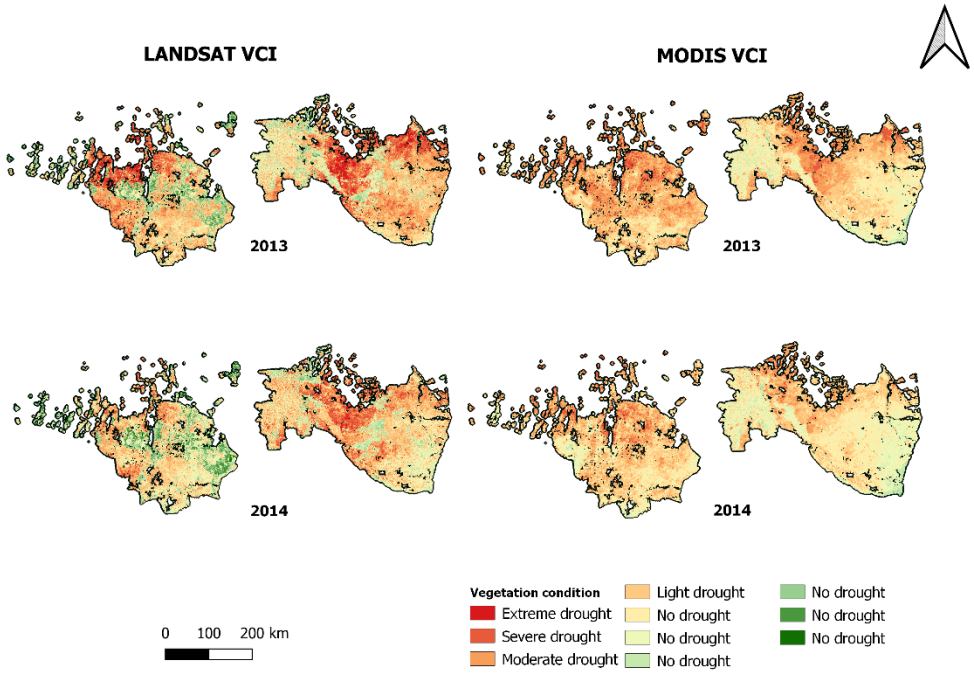

Figure 14. Annual mean VCI using Landsat 7 and MODIS over the study regions during 2013 and 2014

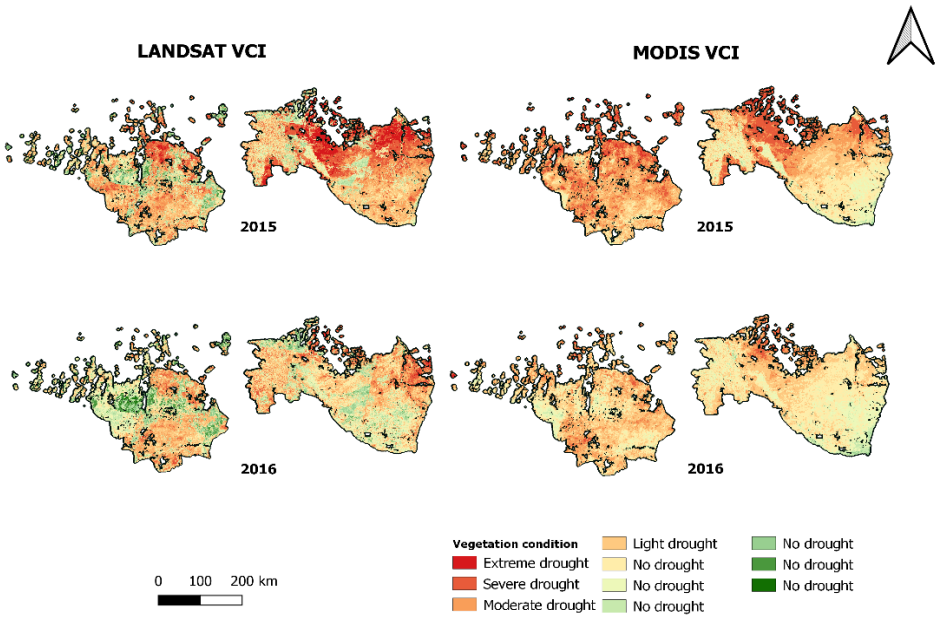

Figure 15. Annual mean VCI using Landsat 7 and MODIS over the study regions during 2015 and 2016

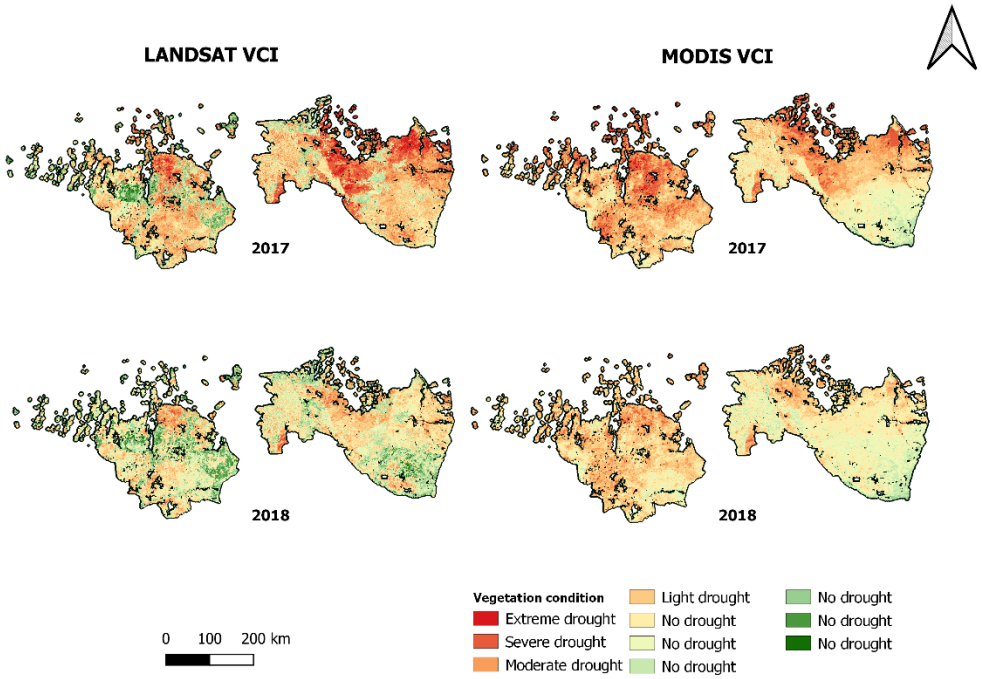

Figure 16. Annual mean VCI using Landsat 7 and MODIS over the study regions during 2017 and 2018

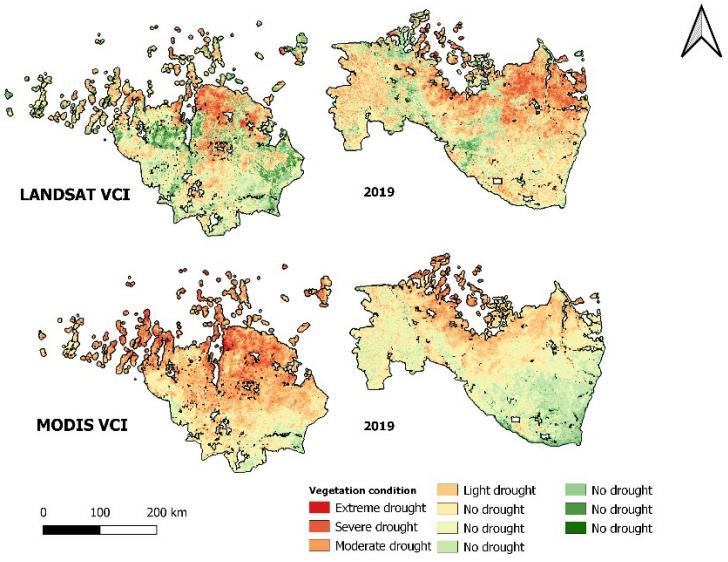

Figure 17. Annual mean VCI using Landsat 7 and MODIS over the study regions during 2019

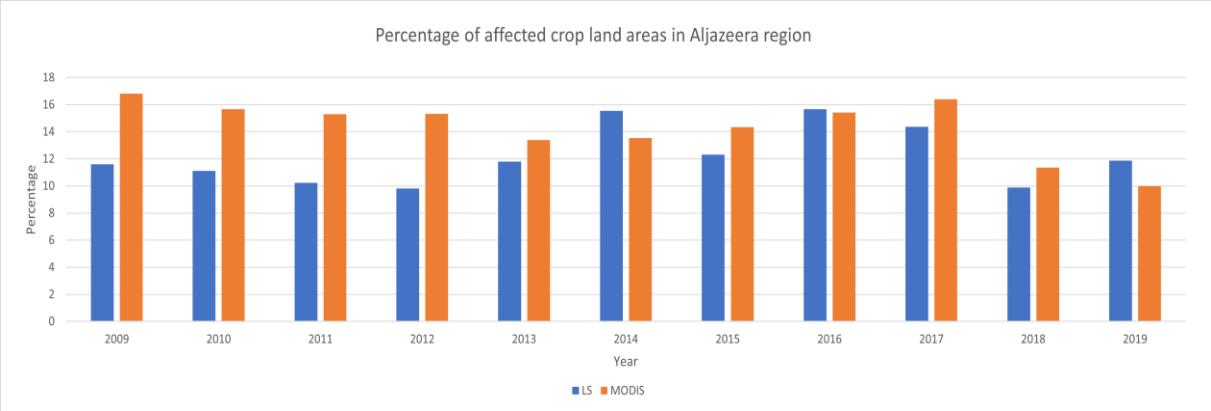

Figure 18. The estimated percentages of the affected cropland in Algazeera region using Landsat 7 and MODIS

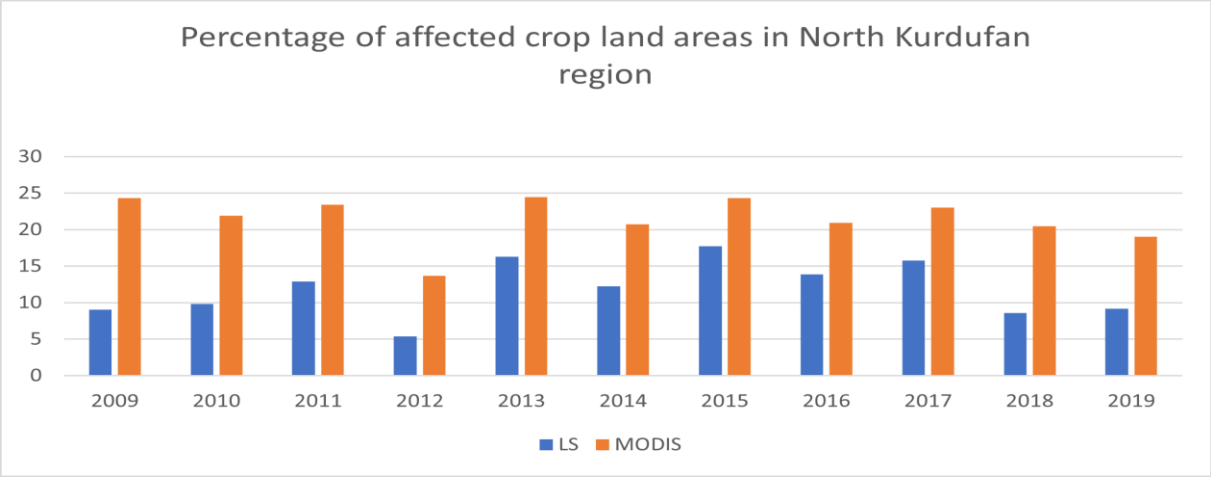

Figure 19. The estimated percentages of the affected cropland in North Kurdufan region using Landsat 7 and MODIS

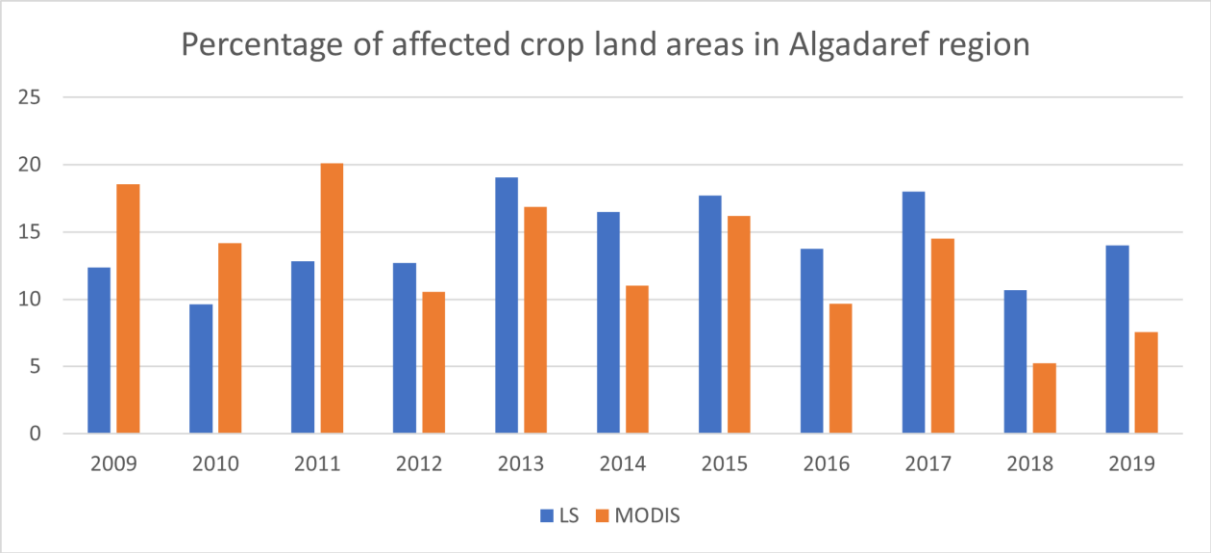

Figure 20. The estimated percentages of the affected cropland in Algadaref region using Landsat 7 and MODIS

4.3 Monthly VCI estimation

As the three most vulnerable years to the agricultural drought were estimated to be 2009, 2011 and 2015, and as was shown by [20], the timing of a drought's start and duration, besides frequency, duration, and intensity, are crucial factors to consider when assessing the impact of drought. Therefore, here we considered the monthly-based VCI maps in these three years when the drought hazard conditions were significantly observed to measure the drought onset and its duration over each season.

Figure 21 and Figure 22 show the monthly vegetation conditions during the agricultural season of 2009 over the study areas using MODIS and Landsat, respectively. According to the MODIS maps, the agricultural season begins with a severe drought on most cropland in June, and then the drought severity is diluted over time to be a moderate drought in July at the majority of the Algazeerah and Algadaref regions, as well as the central part of the North Kurdufan region. Most cropland experiences light or no drought conditions in August, and crop conditions reach a seasonal optimal situation in September.

Likewise, Landsat derived maps described the identical cyclic behaviour of the vegetation condition and its spatial distribution, where the highest spots of the agricultural drought identified by Landsat were very similar to the ones identified by MODIS. A similar outcome was expected considering the VCI's nature and moreover, it confirms the capability of the VCI to characterize the drought conditions. However, the Landsat could detect the vegetation conditions' extremes. We can clearly observe such behaviour in Landsat's June map that shows the overall drought level as an extreme drought and the healthier vegetation condition in September's map compared with the corresponding results of MODIS at the same time, where the June's map shows overall severe drought and less vegetation condition in September's one.

We can generalize the above comments to include the 2011 results (Figure 23, and Figure 24) as the two years were similar and characterized the drought onset to be in

June and continue up to August, then the vegetation condition reaches its maximum in September before it gradually decays in October and November.

On the other hand, the monthly-based VCI maps of 2015 derived from the two sensors as shown in Figure 25 and Figure 26 show that the severe to extreme drought spatial distribution was detected in June and continued to July. However, this season, the vast majority of cropland still experienced moderate and higher drought classes in August. Furthermore, the peak of the vegetation conditions continued during September and October compared with the peak in the other two highest drought years (2009 and 2011) where the peak of the season was in September; this might be interpreted as the peak of the season affected by the drought onset and duration, and as a result, the more intense the drought, as it is reflected in the considerable reduction in the 2015 season crop productivity compared with other seasons as reported by FAO [31].

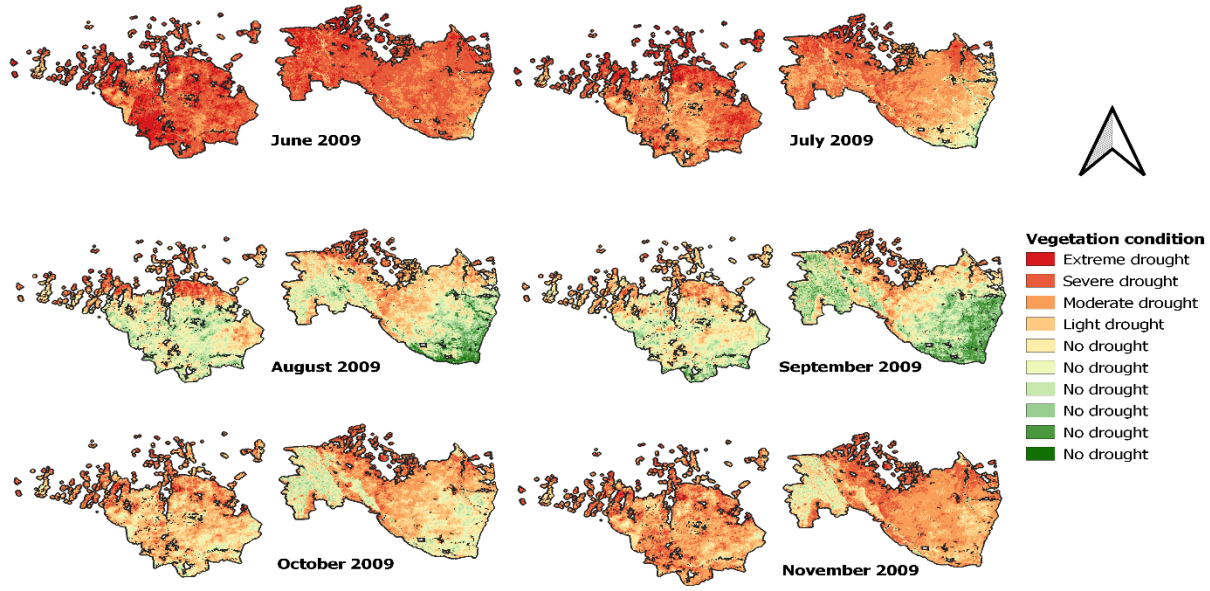

Figure 21. MODIS-based monthly mean VCI during 2009 agricultural season

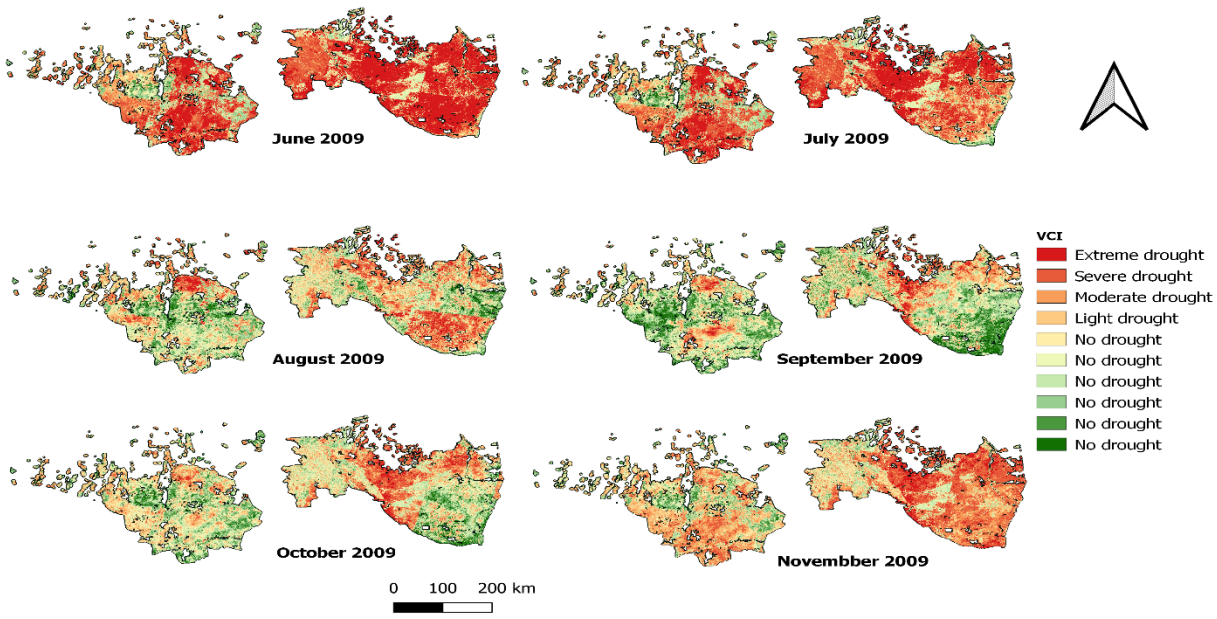

Figure 22. Landsat 7-based monthly mean VCI during 2009 agricultural season

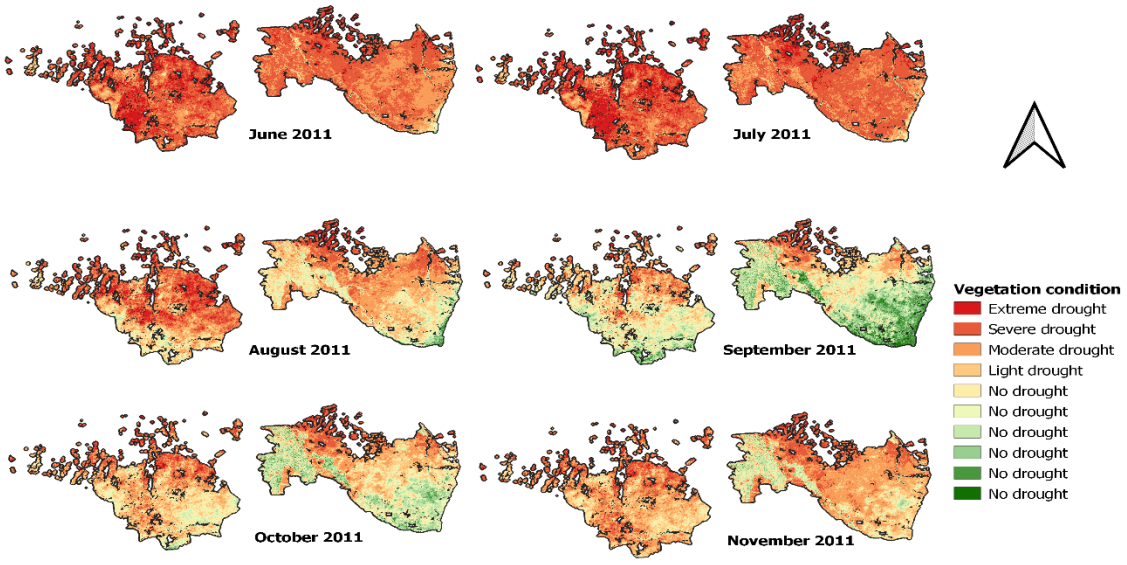

Figure 23. MODIS-based monthly mean VCI during 2011 agricultural season

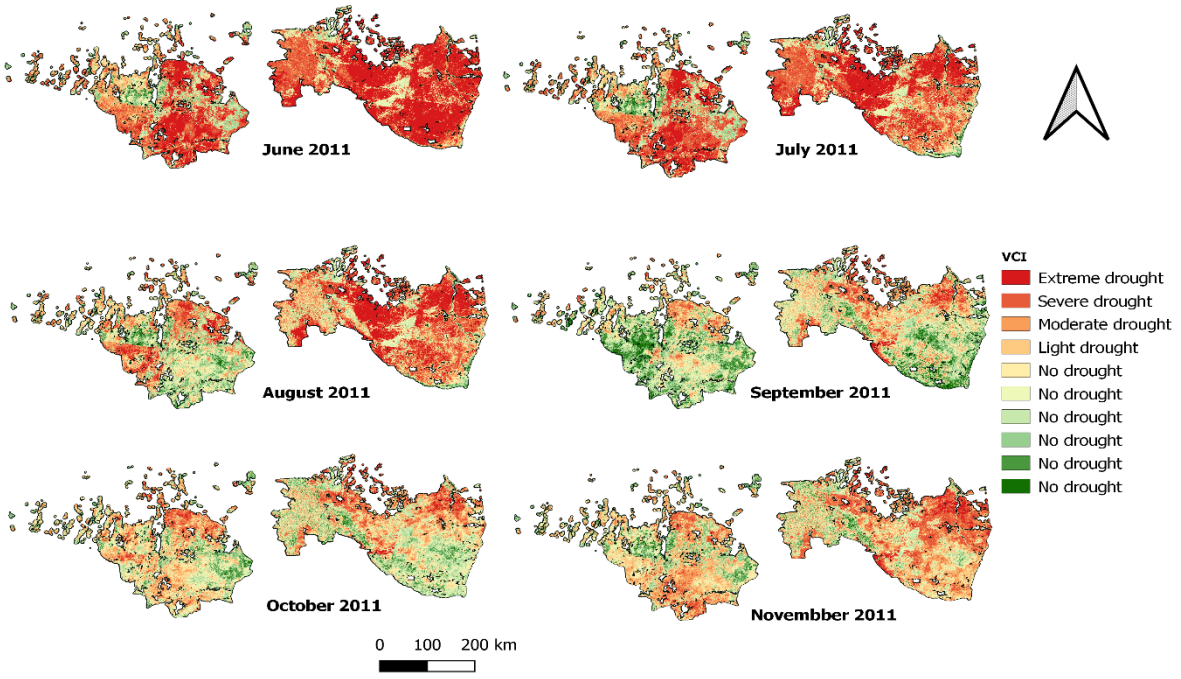

Figure 24. Landsat 7-based monthly mean VCI during 2011 agricultural season

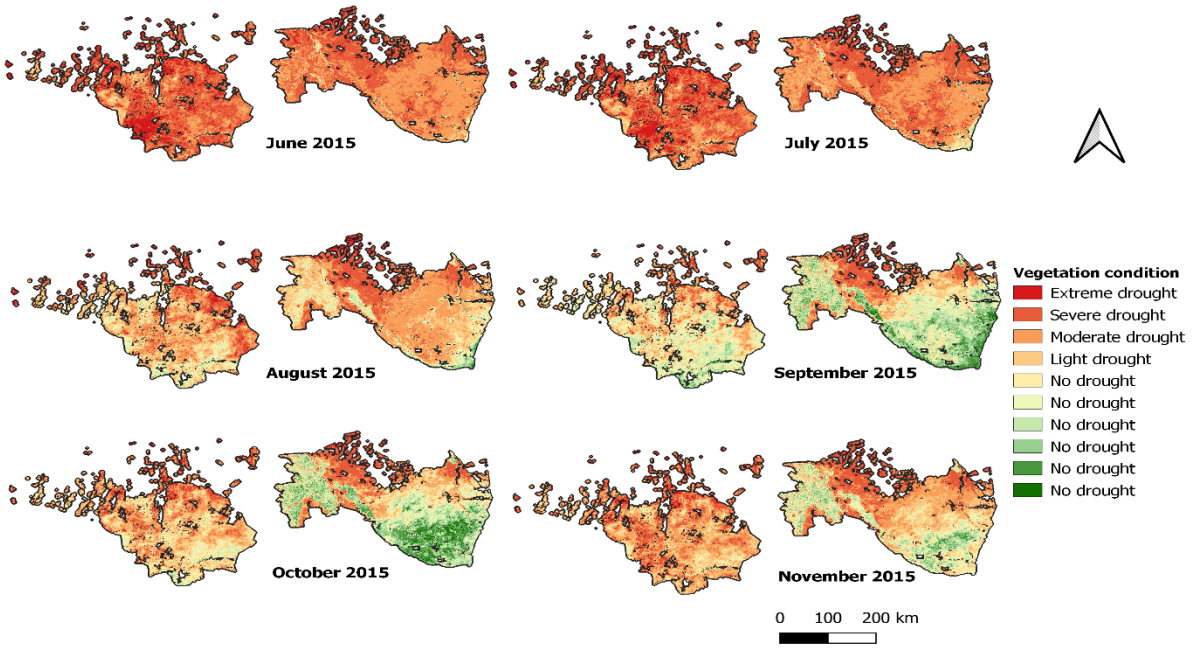

Figure 25. MODIS-based monthly mean VCI during 2015 agricultural season

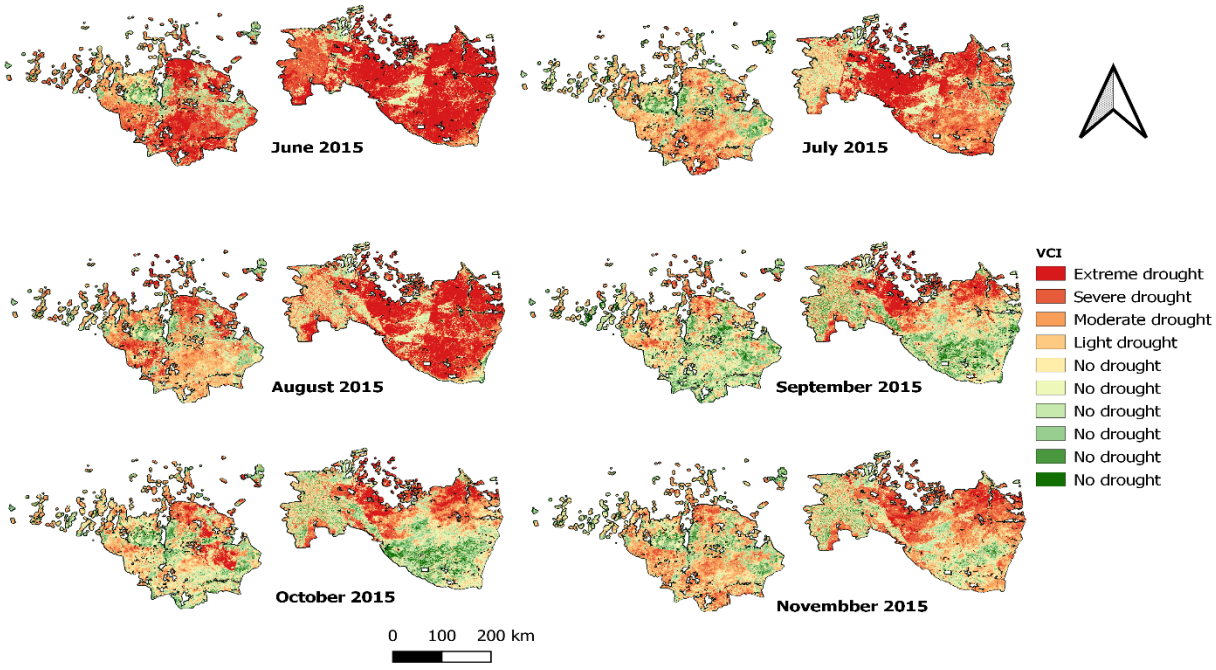

Figure 26. Landsat 7-based monthly mean VCI during 2015 agricultural season

4.5 Drought-counter images

Figure 27 below shows the MODIS and Landsat 7 drought-counter images; images show the aggregated annual drought frequency over time. The images were aimed to identify the most vulnerable areas to the agricultural drought so, they can be used for further analysis in related research and applications. By analyzing the drought spots in the drought-counter images, we can recognize the agreement between the two drought-counter images in identifying the most vulnerable areas to drought as: Sheikan administrative unit in North Kurdufan region, East Algazeera locality in Algazeera region, and Albutana locality in Algadaref region.

The above-mentioned areas were expected to be highlighted as frequently affected regions by drought as they were reported as vulnerable areas to drought by the national plan to mitigate the agricultural hazards [1].

However, the MODIS drought-counter image defined the central parts of North Kurdufan region as vulnerable areas to drought risk while the Landsat classified these areas as non-risky areas to the drought.

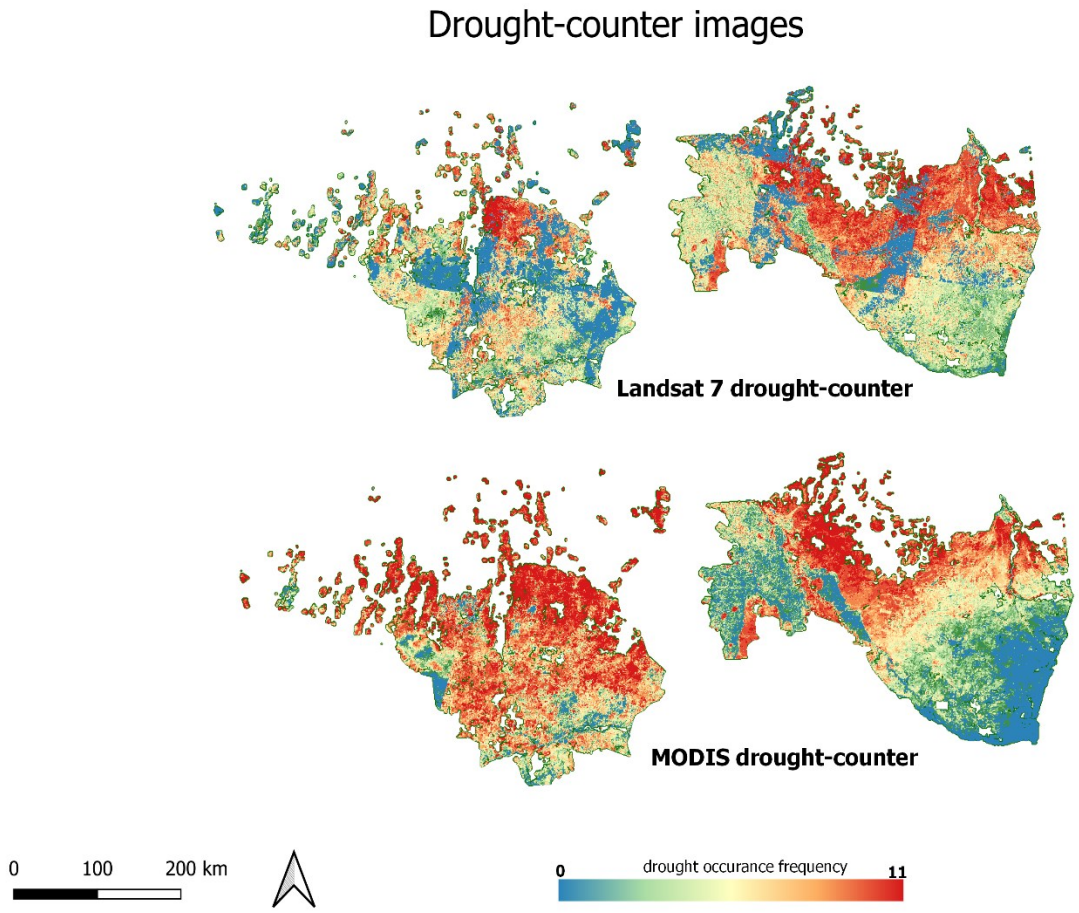

Figure 27. The drought counter images based on Landsat 7 (above) and MODIS (bottom).

4.6 Fused images VCIs results

The Fused images derived VCI maps are mainly implemented to benefit from the advantages of the two sensors (i.e., higher image capturing frequency of MODIS and the finer spatial resolution that the Landsat provides). Using such blended satellite records, the results are expected to show the drought onset with a narrower time range and a detailed drought spatial distribution. Thus, it can be integrated with an early warning system for detecting and monitoring drought.

For evaluating the fused-NDVI records, the correlation between the resulted fused-NDVI records and the MODIS records over the three analyzed regions was estimated. Here, the correlation was evaluated over the same epoch; day of data gathering since the fused-NDVI data had its dates of resampling from the MODIS dataset. While the correlation between the Landsat and the fused data, due to the different temporal resolution of the two datasets, had been estimated between the closest epochs.

The identical trends of MODIS NDVI and the fused-NDVI records (Figure 28,Figure 29, and Figure 30) highlight the suitability and potential of the fused-NDVI to characterize the vegetation condition over the cropland during the study period as well, this confirms the assumption of the linear regression model that describes the relationship between the Landsat and MODIS NDVI made by M. He et al. [2]. Moreover, the strong correlation values between the MODIS and the fused NDVI (0.99 in the Algazeera region, 0.97 in the North Kurdufan region, and 0.98 in the Algadaref region) explained the limitations that the MODIS and Fused derived VCI maps have in emphasizing the extreme vegetation conditions compared with the high sensitivity of the Landsat-based VCIs results in detecting such events.

Figure 31, and Figure 32 show the trends of the Landsat and the fused NDVI records. The corresponding estimated correlation results between the two datasets (0.75 in the Algazeera region, 0.75 in the North Kurdufan region, and 0.87 in the Algadaref region)

provide insight into the reliability of the fused NDVI with respect to the Landsat data, especially in the latest region.

The fused records describe the vegetation condition on an 8-day basis over the cultivation season of 2015. Figure 33 shows the evolution of the drought situation from the 18th of June till the 20th of July. Here, most of the cropland experienced extreme or distributed severe drought. This gives insight that the drought onset was occurred before the determined start of the cultivatioin season. In the next two weeks, the crops condition was improved slightly, and the drought concentration decreased especially in Algazeera and the southern parts of Algadaref region.

By the 5th of August (Figure 34), the central parts of North Kurdufan region, the western and southwest parts of Algadaref, and all of Algazeerah region, the vegetation condition became either light drought or no drought situation. The situation remained from the 5th of August showed till the 29th of August image shows a considerable improvement in the vegetation condition in the overall cropland mask which continued till the 22nd of September where the vegetation condition reached its peak in both Algazeera and North Kurdufan regions, while in Algadaref, the seasonal optimal point was reached in VCI map of the 28th of October (Figure 35). These results confirm the stability of the extracted phenological information from MODIS land dynamics that showed different time intervals of different regions.

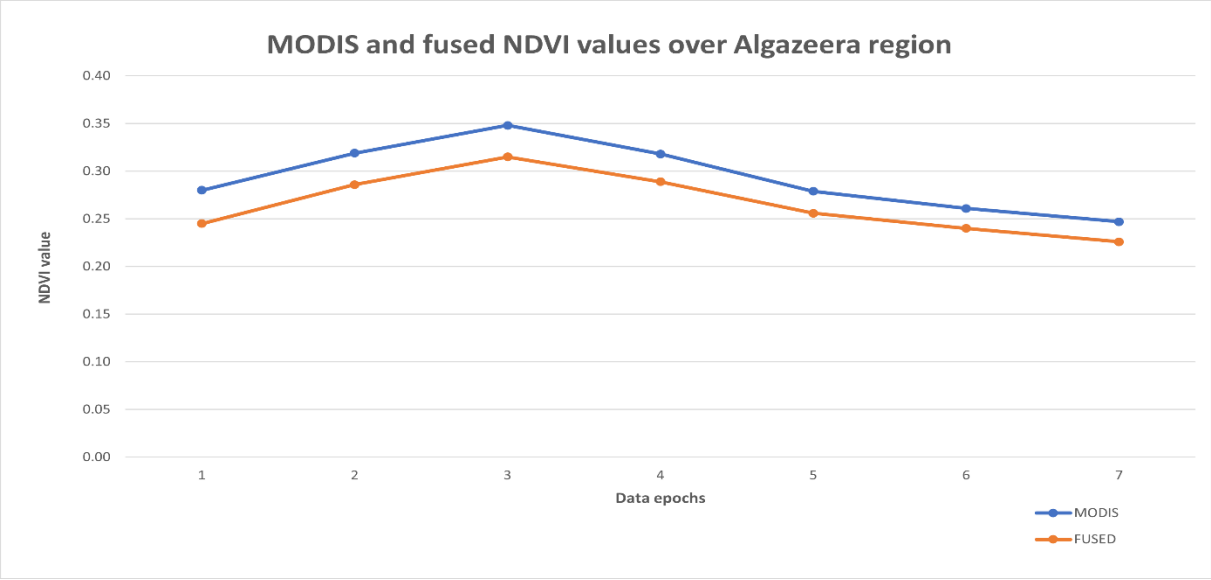

Figure 28. MODIS and fused NDVI values over Algazeera region

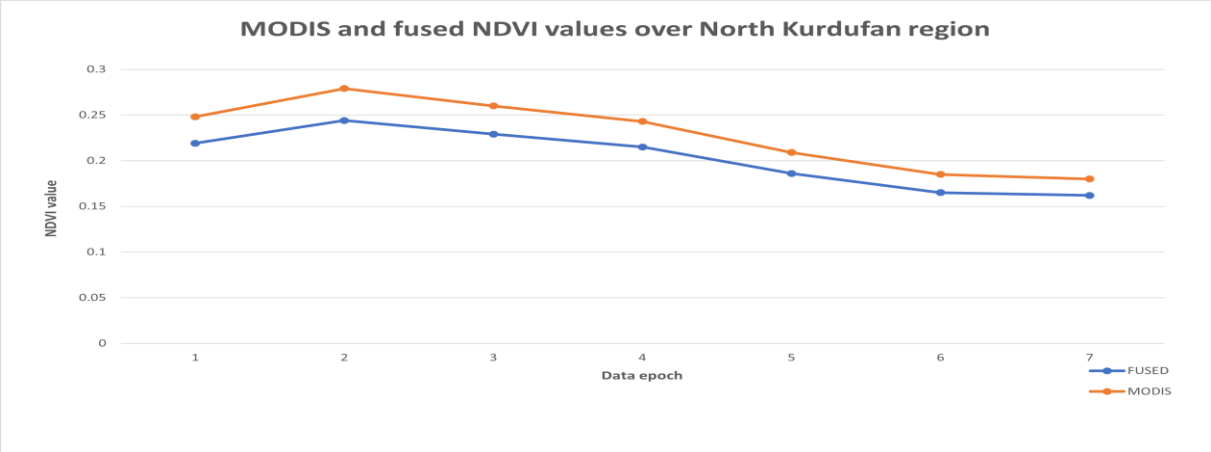

Figure 29. MODIS and fused NDVI values over North Kurdufan region

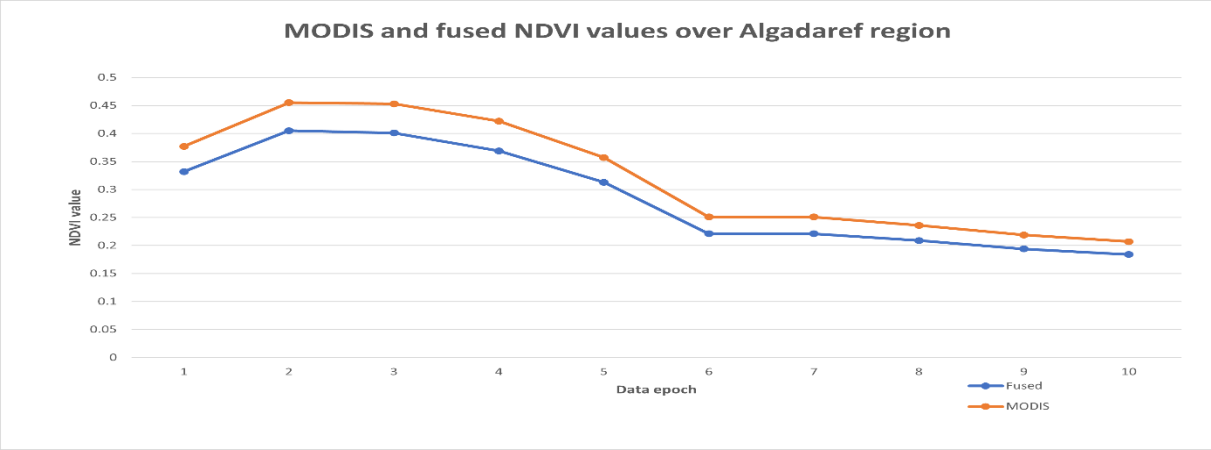

Figure 30. MODIS and fused NDVI values over Algadaref region

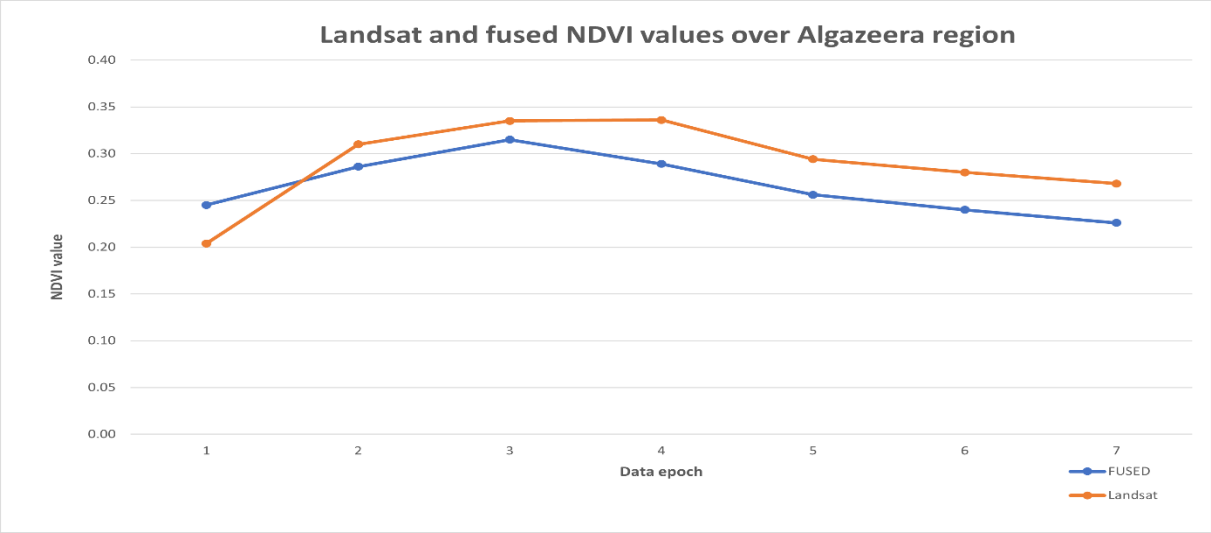

Figure 31. Landsat and fused NDVI values over Algazeera region

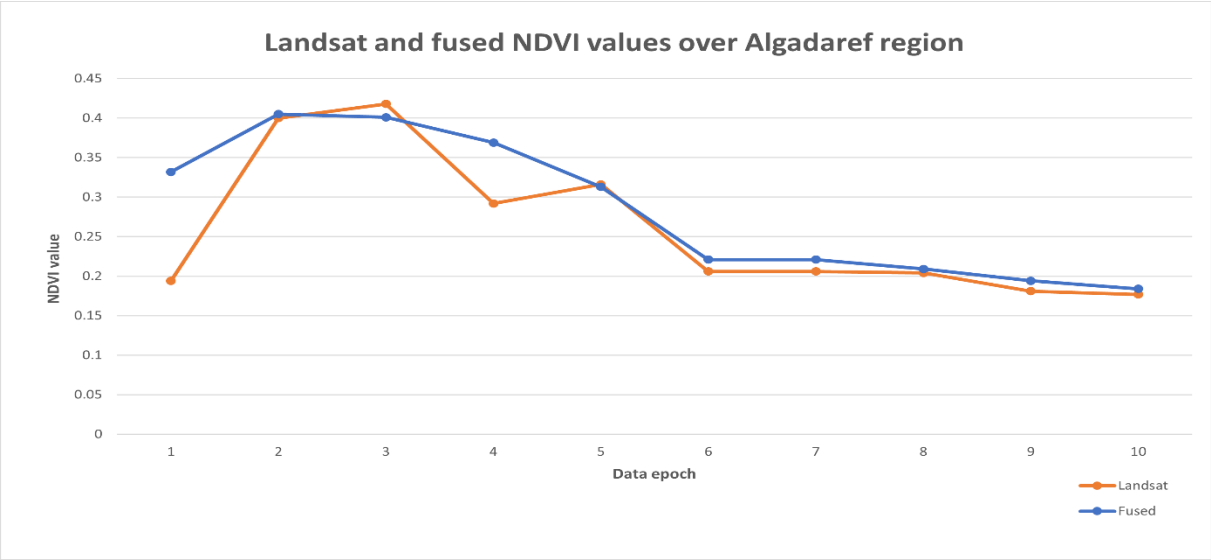

Figure 32. Landsat and fused NDVI values over Algadaref region

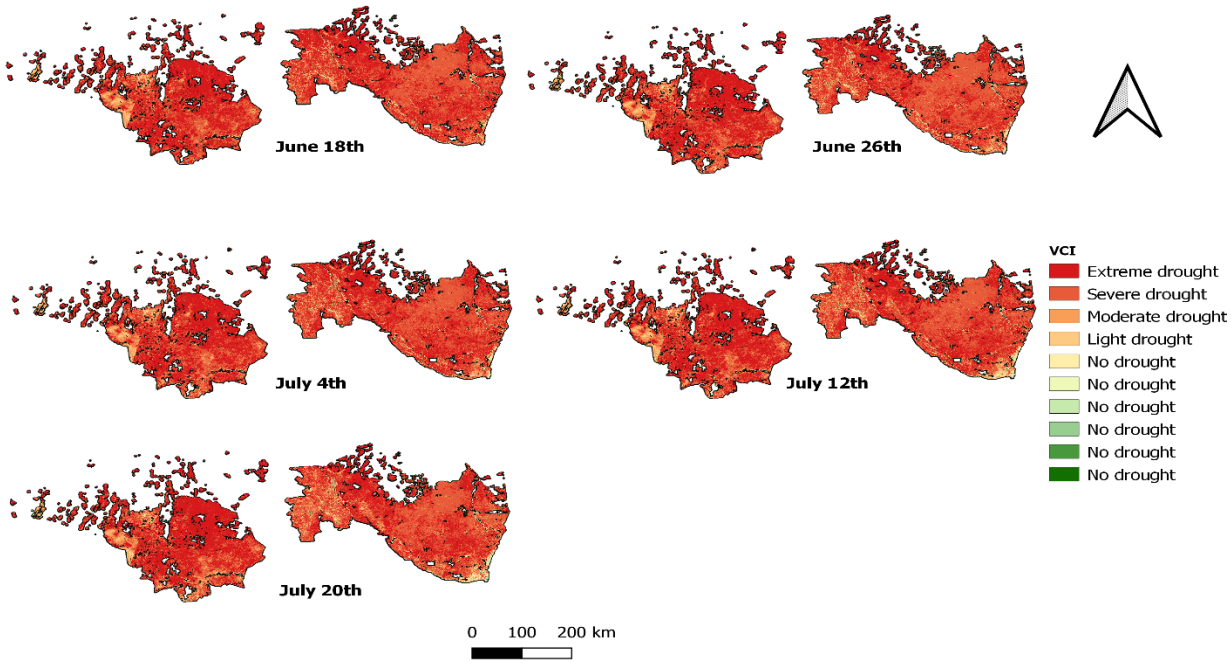

Figure 33. The 8-day fused-based VCI between June 18th and July 20th

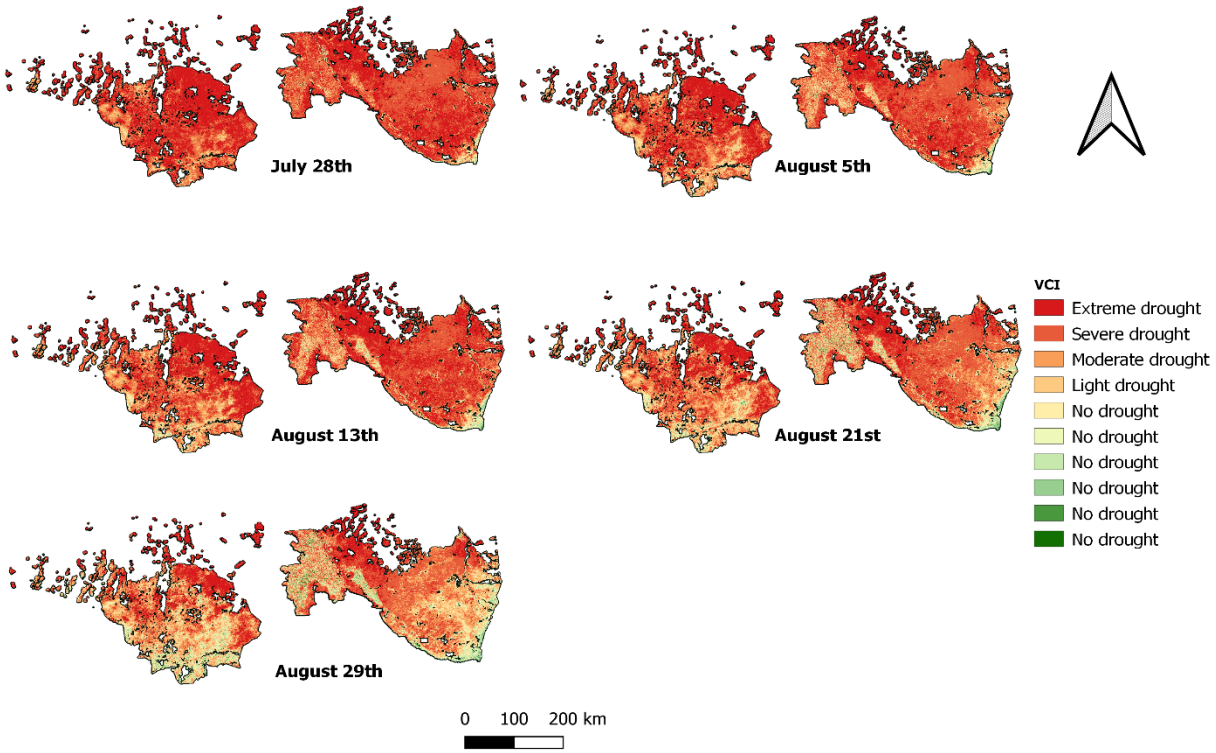

Figure 34. The 8-day fused-based VCI between July 28th and August 29th

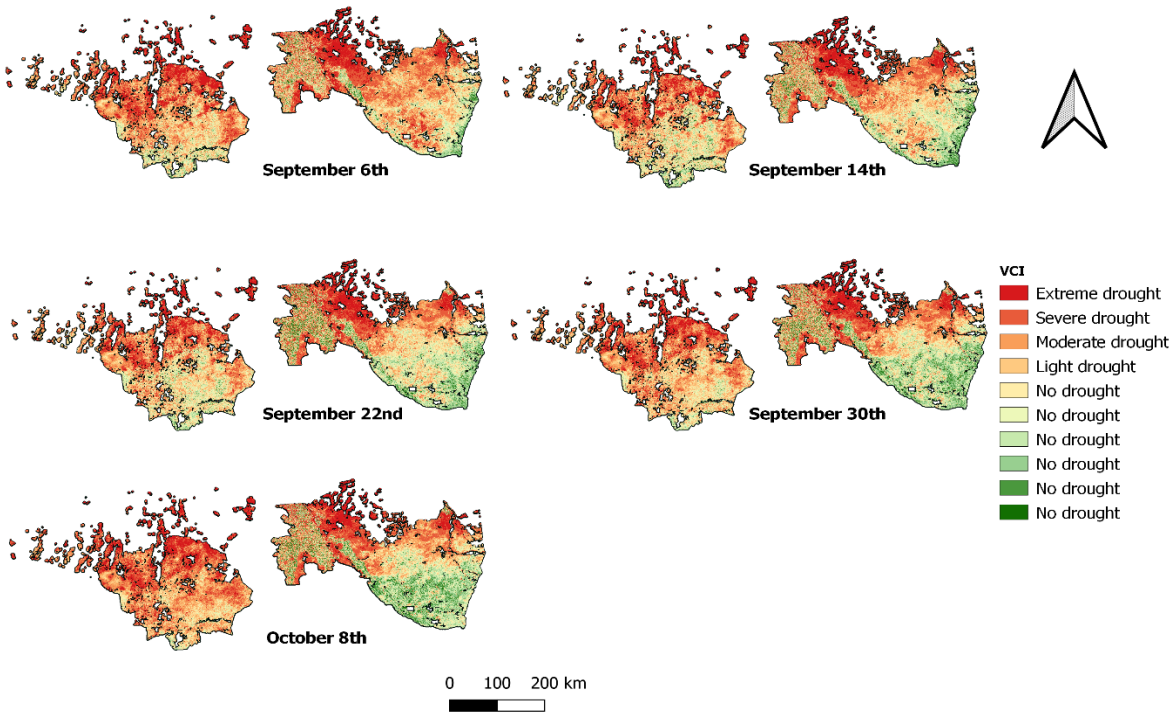

Figure 35. The 8-day fused-based VCI between September 6th and October 8th

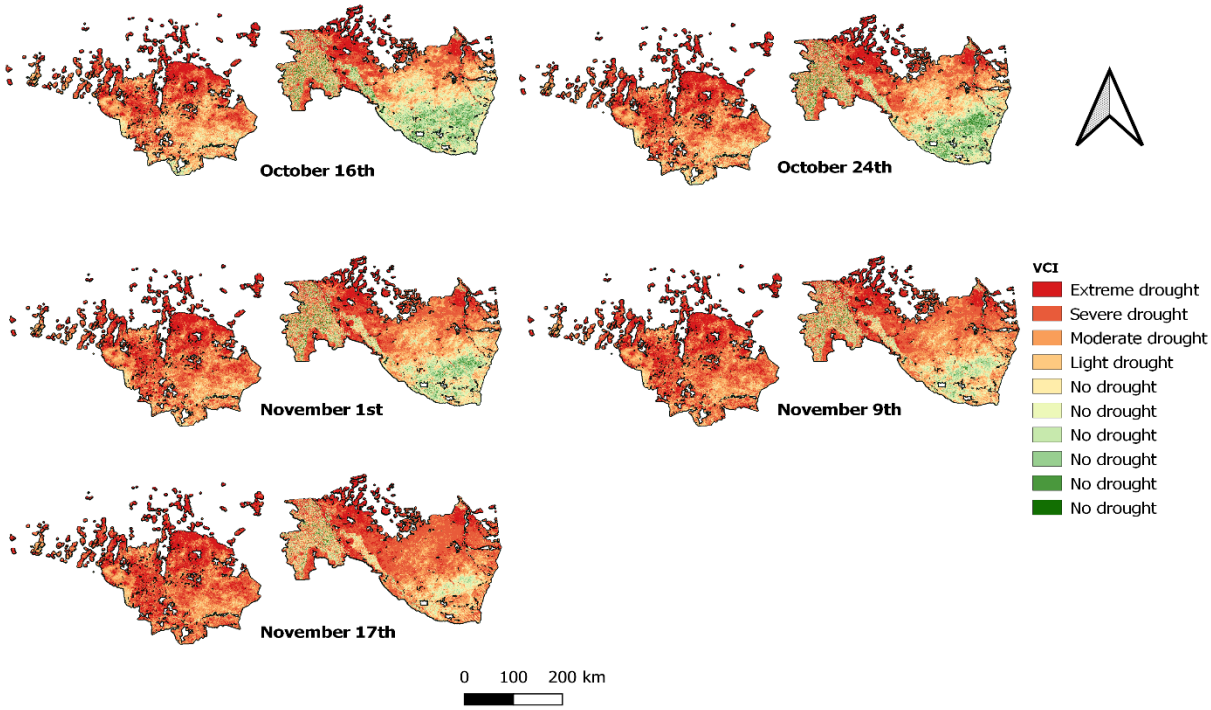

Figure 36. The 8-day fused-based VCI between October 16th and November 17th

By the 24th of October, the cropland areas in North Kurdufan region were became drought areas again while the vegetation in Algadaref and Algazeera experiences no drought till the end of the first decade of November.

The provided fused maps coincide with the monthly-based results shown by MODIS and Landsat for the same agricultural season. However, it can be recognized that the fused data has less sensitivity to the vegetation extremes compared with the maps generated from Landsat observations. This can be attributed to the higher correlation between the fused data and the MODIS one when compared with the correlation between the fused data and the Landsat ones and because of the higher spectral resolution that the Landsat 7 has.

Generally, the produced maps from the fused data coincided with the monthly-based VCI maps of MODIS and Landsat and showed the success of the derived VCI from the fused dataset in describing the temporal evolution of the drought and the vegetation condition over time. Moreover, the fused data emphasized the spatial pattern of the drought distribution over the cropland that the two original sensors identified.

4.7 Affected population by the agricultural drought

The affected population by the agricultural drought was estimated thanks to the WorldPop data over the three analyzed regions. Figure 37 below shows the increase in the population in the three regions. While Figure 38 gives information about the percentage of the estimated affected population in each region.

The affected percentages of the population over the study period have fluctuated between 3% to 5% of the total population in the Algazeera and Algadaref regions and between 1.5% to 4.5% for the North Kurdufan region.

The relatively low percentages of the affected population with respect to the estimated percentages of the affected cropland areas indicate the lower density of population in the affected areas. This information reflects the rapid immigration of the population from the rural areas toward the big cities as reported by the national and international reports.

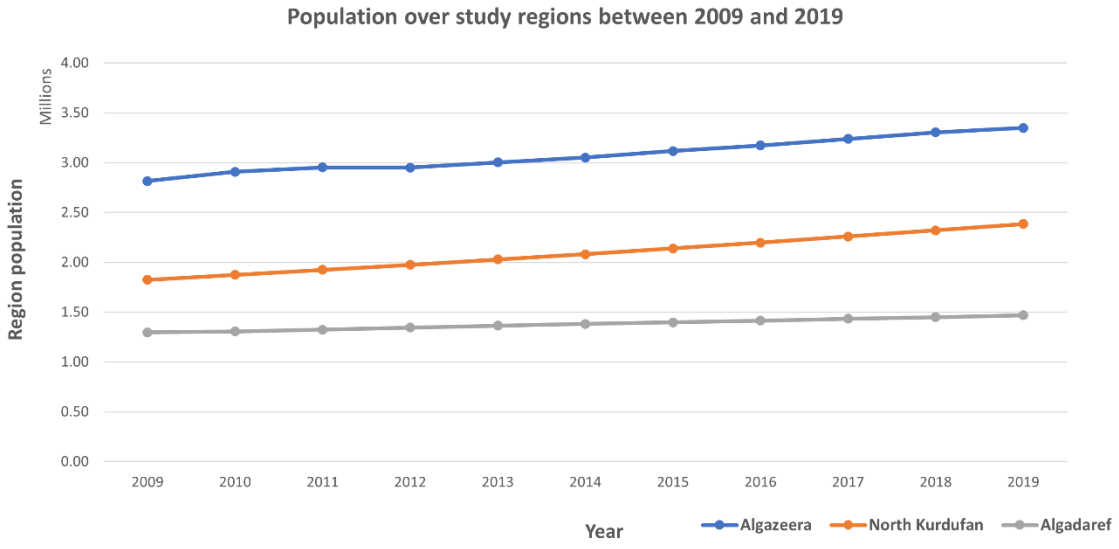

Figure 37. The population over the three study regions between 2009 and 2019

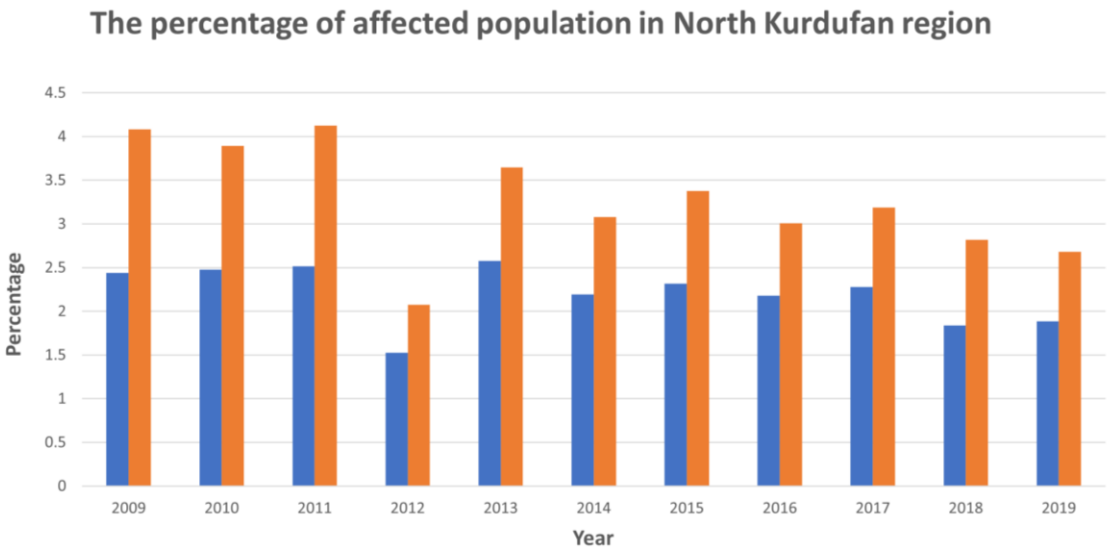

Figure 38. The percentage of the affected population in North Kurdufan region

5. Conclusion and future improvements

In this chapter, a summary of the conducted work and the conclusions of the study will be addressed. Furthermore, the limitations that face the work will be shown as well as the proposed future improvements.

5.1 Conclusions

- The main objective of this study was to characterize the spatial and temporal pattern of the agricultural drought in the irrigated and rainfed cropland in Sudan during the cultivation seasons over the period from 2009 to 2019 using Landsat 7 and MODIS optical satellite-based observations.

- For the above-mentioned purpose, multiple remote sensing datasets were utilized. The MODIS land dynamics dataset was used in identifying the agricultural season duration, and the results showed its capability to determine the agricultural season's start, length, and duration.

- The Landsat 7 and MODIS surface reflectance observations were used to develop the vegetation condition index (VCI) over the study regions. The VCI was implemented on an annual and monthly basis. The obtained results confirmed the index maps' ability to describe the various agricultural drought characteristics (onset, duration, intensity, and frequency) across the study areas. However, the results highlighted the potential of the Landsat 7 based index to detect extreme vegetation conditions spatially and temporally.

- A fused NDVI record was generated thanks to an empirical linear regression model blending spectral information from overlapped Landsat 7 and MODIS observations to overcame the limitations of the original sensors and benefited from their finer resolution (30m spatial resolution and 8-day temporal

resolution). The VCI derived from the fused data showed drought characteristics that were consistent with the information from Landsat and MODIS sensors, with the drought in higher temporal resampling and the ability to be integrated with an early warning system for drought detection and monitoring.

- The results emphasized that the 2009, 2011, and 2015 seasons were the most affected by the drought, while the 2012, 2016, and 2018 seasons experienced the least drought intensity. As a reference for understanding agricultural drought frequency and the vulnerable sites and assisting in future policymaking, an accumulated drought-counter image for each of the two sensors was created. The most vulnerable locations in the counter images were consistent with the local authorities' reports.

- In terms of the affected population, the percentage of the annual vulnerable population was less than 5% in each of the three regions, and the vast majority of them were in rural areas.

5.2 Limitations and future improvements

- The relatively low temporal resolution of the Landsat 7 despite of its reliable spatial resolution was acting as a barrier for early detection and/ or rapidly monitoring of the agricultural drought over the study area.

- The lack of ground truth data about the drought characteristics, in addition to the hardness of access to the local information about the agricultural data, especially in the rainfed cultivation regions, was one of the biggest issues that faced the study. Moreover, most of the local accessible sources were suffering from a lack of continuous updates, which made the temporal information needed for the evaluation incomplete.

- The high time required to process the fusion data compared with the process time needed for elaporating MODIS and Landsat introduces a challenge for using this data for analyzing agriculture over a long period of analysis. One proposed future improvement is to generate a continuously updated fused record from the newly acquired MODIS and Landsat data so that it is ready to use in the Google Earth Engine.

Bibliography

[1] "REPUBLIC OF THE SUDAN Ministry of Environment, Natural Resources& Physical Development Higher Council for Environment and Natural Resources National AdaptationPlan," 2016.

[2] M. He *et al.*, "Regional crop gross primary productivity and yield estimation using fused landsat-MODIS data," *Remote Sens.*, vol. 10, no. 3, 2018, doi: 10.3390/rs10030372.

[3] J. Ren, Z. Chen, Q. Zhou, and H. Tang, "Regional yield estimation for winter wheat with MODIS-NDVI data in Shandong , China," *Int. J. Appl. Earth Obs. Geoinf.*, vol. 10, no. 4, pp. 403–413, 2008, doi: 10.1016/j.jag.2007.11.003.

[4] D. B. Lobell, "Field Crops Research The use of satellite data for crop yield gap analysis," *F. Crop. Res.*, vol. 143, pp. 56–64, 2013, doi: 10.1016/j.fcr.2012.08.008.

[5] F. N. Kogan, "Droughts of the Late 1980s in the United States as Derived from NOAA Polar-Orbiting Satellite Data."

[6] G. Ghazaryan, S. König, E. E. Rezaei, S. Siebert, and O. Dubovyk, "Analysis of drought impact on croplands from global to regional scale: A remote sensing approach," *Remote Sens.*, vol. 12, no. 24, pp. 1–17, Dec. 2020, doi: 10.3390/rs12244030.

[7] O. Dubovyk, G. Ghazaryan, J. González, V. Graw, F. Löw, and J. Schreier, "Drought hazard in Kazakhstan in 2000–2016: a remote sensing perspective," *Environ. Monit. Assess.*, vol. 191, no. 8, 2019, doi: 10.1007/s10661-019-7620-z.

[8] G. Venuti, "Lecture notes in Earth Observations," 2021.

[9] C. Technology, "Satellite remote sensing for conservation".

[10] D. Series, "USGS Spectral Library Version 7 Data Series 1035".

[11] J. Gray, D. Sulla-Menashe, and M. A. Friedl, "User Guide to Collection 6 MODIS Land Cover Dynamics (MCD12Q2) Product," 2019.

[12] T. P. et Al., *Global Food Security Support Analysis Data at Nominal 1 km (GFSAD1km) Derived from Remote Sensing in Support of Food Security in the Twenty-First Century: Current Achievements and Future Possibilities*. 2005.

[13] H. Tamiminia, B. Salehi, M. Mahdianpari, L. Quackenbush, S. Adeli, and B. Brisco, "Google Earth Engine for geo-big data applications: A meta-analysis and systematic review," *ISPRS Journal of Photogrammetry and Remote Sensing*, vol. 164.

Elsevier B.V., pp. 152–170, Jun. 01, 2020. doi: 10.1016/j.isprsjprs.2020.04.001.

[14] M. Amani *et al.*, "Google Earth Engine Cloud Computing Platform for Remote Sensing Big Data Applications: A Comprehensive Review," *IEEE J. Sel. Top. Appl. Earth Obs. Remote Sens.*, vol. 13, pp. 5326–5350, 2020, doi: 10.1109/JSTARS.2020.3021052.

[15] L. Kumar and O. Mutanga, "Google Earth Engine applications since inception: Usage, trends, and potential," *Remote Sens.*, vol. 10, no. 10, Oct. 2018, doi: 10.3390/rs10101509.

[16] L. Mutanga, O.; Kumar, "Google Earth Engine Applications," pp. 11–14, 2019, doi: 10.3390/rs11050591.

[17] M. A. Brovelli, Y. Sun, and V. Yordanov, "Monitoring forest change in the amazon using multi-temporal remote sensing data and machine learning classification on Google Earth Engine," *ISPRS Int. J. Geo-Information*, vol. 9, no. 10, Oct. 2020, doi: 10.3390/ijgi9100580.

[18] N. Gorelick, M. Hancher, M. Dixon, S. Ilyushchenko, D. Thau, and R. Moore, "Google Earth Engine : Planetary-scale geospatial analysis for everyone," *Remote Sens. Environ.*, vol. 202, pp. 18–27, 2017, doi: 10.1016/j.rse.2017.06.031.

[19] N. E. Young, R. Anderson, S. Chignell, and A. Vorster, "A survival guide to Landsat preprocessing," no. March, 2017, doi: 10.1002/ecy.1730.

[20] V. Graw *et al.*, "Timing is Everything-Drought Classification for Risk Assessment," *IEEE J. Sel. Top. Appl. Earth Obs. Remote Sens.*, vol. 13, pp. 428–433, 2020, doi: 10.1109/JSTARS.2019.2963576.

[21] X. Zhang, M. A., B. Tan, M. D., and Y. Yu, "Long-Term Detection of Global Vegetation Phenology from Satellite Instruments," *Phenol. Clim. Chang.*, no. May 2014, 2012, doi: 10.5772/39197.

[22] S. Huang, L. Tang, J. P. Hupy, Y. Wang, and G. Shao, "A commentary review on the use of normalized difference vegetation index (NDVI) in the era of popular remote sensing," *Journal of Forestry Research*, vol. 32, no. 1. Northeast Forestry University, Feb. 01, 2021. doi: 10.1007/s11676-020-01155-1.

[23] R. W. H. Rouse, J. A. W. Haas, and D. W. Deering, "'aper A 20 MONITORING VEGETATION SYSTEMS IN THE GREAT PLAINS WITH ERTS."

[24] F. Gao *et al.*, "Fusing Landsat and MODIS Data for Vegetation Monitoring," *IEEE Geosci. Remote Sens. Mag.*, vol. 3, no. 3, pp. 47–60, 2015, doi: 10.1109/MGRS.2015.2434351.

[25] T. Hilker *et al.*, "Generation of dense time series synthetic Landsat data through

data blending with MODIS using a spatial and temporal adaptive reflectance fusion model," *Remote Sens. Environ.*, vol. 113, no. 9, pp. 1988–1999, 2009, doi: 10.1016/j.rse.2009.05.011.

[26] J. Ju and D. P. Roy, "The Availability of Cloud-free Landsat ETM + Data Over the Conterminous U . S . and Globally The availability of cloud-free Landsat ETM + data over the conterminous United States and globally," no. March 2014, 2007, doi: 10.1016/j.rse.2007.08.011.

[27] "Vegetation index for aerial analysis of crop conditions," *Proc. 18th Conf. Agric. For. Meteorol.*, no. AMS, W. Lafayette, Indiana, on 15–18 September (Indiana, USA), pp. 103–106, 1987.

[28] Y. Han *et al.*, "Monitoring droughts in the greater changbai mountains using multiple remote sensing-based drought indices," *Remote Sens.*, vol. 12, no. 3, Feb. 2020, doi: 10.3390/rs12030530.

[29] C. Bhuiyan, R. P. Singh, and F. N. Kogan, "Monitoring drought dynamics in the Aravalli region (India) using different indices based on ground and remote sensing data," *Int. J. Appl. Earth Obs. Geoinf.*, vol. 8, no. 4, pp. 289–302, 2006, doi: 10.1016/j.jag.2006.03.002.

[30] P. S. Thenkabail, M. S. D. N. Gamage, V. Smakhtin, and International Water Management Institute., *The use of remote sensing data for drought assessment and monitoring in southwest Asia*. International Water Management Institute, 2004.

[31] FAO, "FAO STAT," *FAO.[FAOSTAT]. License: CC BY-NC-SA 3.0 IGO. Extracted from: [https://www.fao.org/faostat/en/#data/QCL]. Data of Access: [15-05-2022].*

List of Figures

List of Tables

2. Acknowledgements

I would like to thank my supervisor Prof. Maria Antonia Brovelli for her genuine support and valuable advice and guides and for giving me the time and knowledge. Her constructive criticism and insightful comments have surely assisted me to achieve this dissertation. None of this work can done without her pieces of advice.

I would like also to express my gratitude to the people who made significant contributions to my life, my beloved parents, I cannot repay them for their invaluable love and support since the day I was conceived on this Earth as well as my brother and sisters for their unwavering support, trust and love always pushing us forward.

Last but not least, thanks to all my friends for their authentic support. As I should restate that I would like to thank all of those who supported me in any respect during the completion of my study and any aspects of life and to express our apology for not mentioning them by name.